water

MDPI

Article

Estimation of Potential Soil Erosion and Sediment Yield: A Case Study of the Transboundary Chenab River Catchment

Muhammad Gufran Ali [1], Sikandar Ali [1,*], Rao Husnain Arshad [1], Aftab Nazeer [2,3,*], Muhammad Mohsin Waqas [4], Muhammad Waseem [5], Rana Ammar Aslam [6], Muhammad Jehanzeb Masud Cheema [7], Megersa Kebede Leta [8] and Imran Shauket [6]

1 Department of Irrigation and Drainage, Faculty of Agricultural Engineering and Technology, University of Agriculture, Faisalabad 38000, Pakistan; mgufranali008@gmail.com (M.G.A.); husnain.arshad@uaf.edu.pk (R.H.A.)
2 Department of Water Management, Delft University of Technology, 2600 GA Delft, The Netherlands
3 Department of Agricultural Engineering, Bahauddin Zakariya University, Multan 60800, Pakistan
4 Department of Agricultural Engineering, Khwaja Fareed University of Engineering and Information Technology, Rahim Yar Khan 64200, Pakistan; mohsin.waqas@kfueit.edu.pk
5 Department of Civil Engineering, Ghulam Ishaq Khan Institute of Engineering Sciences and Technology, Topi 23460, Pakistan; muhammad.waseem@giki.edu.pk
6 Department of Structures and Environmental Engineering, Faculty of Agricultural Engineering and Technology, University of Agriculture, Faisalabad 38000, Pakistan; ammar.aslam@uaf.edu.pk (R.A.A.); imranshaukat@uaf.edu.pk (I.S.)
7 Department of Land and Water Conservation Engineering, Faculty of Agricultural Engineering and Technology, PMAS Arid Agriculture University, Rawalpindi 46000, Pakistan; mjm.cheema@uaar.edu.pk
8 Faculty of Agriculture and Environmental Sciences, University of Rostock, 18059 Rostock, Germany; megersa.kebede@uni-rostock.de
* Correspondence: sikandar_ali@uaf.edu.pk (S.A.); a.nazeer@tudelft.nl (A.N.); Tel.: +92-3217659581 (S.A.); +31-649065653 (A.N.)

Citation: Ali, M.G.; Ali, S.; Arshad, R.H.; Nazeer, A.; Waqas, M.M.; Waseem, M.; Aslam, R.A.; Cheema, M.J.M.; Leta, M.K.; Shauket, I. Estimation of Potential Soil Erosion and Sediment Yield: A Case Study of the Transboundary Chenab River Catchment. *Water* **2021**, *13*, 3647. https://doi.org/10.3390/w13243647

Academic Editors: Csaba Centeri

Received: 25 October 2021
Accepted: 15 December 2021
Published: 18 December 2021

Abstract: Near real-time estimation of soil loss from river catchments is crucial for minimizing environmental degradation of complex river basins. The Chenab river is one of the most complex river basins of the world and is facing severe soil loss due to extreme hydrometeorological conditions, unpredictable hydrologic response, and complex orography. Resultantly, huge soil erosion and sediment yield (SY) not only cause irreversible environmental degradation in the Chenab river catchment but also deteriorate the downstream water resources. In this study, potential soil erosion (PSE) is estimated from the transboundary Chenab river catchment using the Revised Universal Soil Loss Equation (RUSLE), coupled with remote sensing (RS) and geographic information system (GIS). Land Use of the European Space Agency (ESA), Climate Hazards Group InfraRed Precipitation with Station (CHIRPS) data, and world soil map of Food and Agriculture Organization (FAO)/The United Nations Educational, Scientific and Cultural Organization were incorporated into the study. The SY was estimated on monthly, quarterly, seasonal, and annual time-scales using sediment delivery ratio (SDR) estimated through the area, slope, and curve number (CN)-based approaches. The 30-year average PSE from the Chenab river catchment was estimated as 177.8, 61.5, 310.3, 39.5, 26.9, 47.1, and 99.1 tons/ha for annual, rabi, kharif, fall, winter, spring, and summer time scales, respectively. The 30-year average annual SY from the Chenab river catchment was estimated as 4.086, 6.163, and 7.502 million tons based on area, slope, and CN approaches. The time series trends analysis of SY indicated an increase of 0.0895, 0.1387, and 0.1698 million tons per year for area, slope, and CN-based approaches, respectively. It is recommended that the areas, except for slight erosion intensity, should be focused on framing strategies for control and mitigation of soil erosion in the Chenab river catchment.

Keywords: RUSLE; soil erosion; sediment yield; Chenab river; remote sensing; GIS

1. Introduction

Soil is a precious natural resource [1], plays a key role in the functioning ecosystem [2,3], and provides valuable goods and services [4,5] essential for human security [6,7]. Soil erosion is a natural geomorphic process and environmental problem [8,9] arising from anthropogenic activities [10] agricultural intensification, deforestation, land degradation, and global climate change [11,12]. Soil erosion is also considered as one of the significant threats to the ecosystem [13–15], as it not only causes soil erosion from upper catchments and deposition in rivers and lakes through the geologic ages worldwide [16,17], but also carries nutrients, pesticides, chemicals, etc., and cause groundwater contamination [18–20]. It has been estimated that about 56% of global soil is being degraded by light to severe forms of soil erosion caused has by water [21]. Accelerated forms of soil erosion by water become a global problem [22,23], that not only cause rivers' catchment problems [24,25] but also act as barriers to achieving the United Nations Sustainable Development Goals [26]. Therefore, estimation of soil erosion by water from river catchment is in dire need [27], so that proper soil erosion mitigation options can be focused [28].

Estimation of soil erosion (PSE and SY) from large and complex rivers' catchments has always been a big challenge to researchers worldwide [6,29–31]. Initially, soil erosion research was conducted more than seven decades ago using north American datasets [32–34]. Several mathematical models, conceptual, empirical, process oriented, and physically based, have been applied for soil erosion modeling/ estimation at different spatiotemporal scales [35–42]. Scientists are also working on process-oriented soil erosion models such as the Water Erosion Prediction Project [43,44], European Soil Erosion Model [45], Limburg Soil Erosion Model [46], and Pan European Soil Erosion Risk Assessment [47]. The research community is also improving the empirical model known as Universal Soil Loss Equation (USLE) [48–52] which is not only practically sound [53,54] but can also be applied over complex and large river basins [11,55–57]. The USLE and RUSLE are being applied successfully for estimation of PSE and SY from rivers' catchments throughout the world under changing spatiotemporal conditions [6,58–63]. Large-scale soil erosion modeling has been performed by using the RUSLE model in Europe [64], Canada [65], Australia [66], and China [67].

The RUSLE was developed to estimate soil erosion by water in temperate climates, and is an empirical model founded on the USLE [68]. The RUSLE model estimates the average annual rate of soil erosion from complex river basins for multiple scenarios including management practices, cropping systems, and erosion control practices [69]. The RUSLE can also be used for estimation of average annual soil erosion rate from ungauged river catchments using local hydrometeorological information and catchment characteristics [70]. The RUSLE model considers the effect of many factors such as rainfall erosivity, soil erodibility, slope length and slope steepness, cover management, and conservation practices [71]. The soil loss occurs in three steps. Soil erosion starts with the detachment of soil particles, followed by transport and sequent deposition [72]. The RUSLE model neither estimates gully/channel erosion nor discusses the sediment deposition, so there is a need to introduce SDR for estimation of sediment delivered to the outlet from the catchment [73]. The SDR is estimated by researchers based on area, slope, and CN approaches in rivers' catchments globally [74–79]. The RUSLE model is applied along with the SDR for estimation of sediment yield from rivers' catchments [80–84].

The use of RUSLE for soil erosion needs detailed spatiotemporal in situ data [85] which is not possible, as the transboundary Chenab river catchment is divided among Pakistan (402 km^2), Jammu and Kashmir (20,139.7 km^2), and India (7939.27 km^2) [86]. This clearly reflects that 27.87%, 70.71%, and 1.42% area of the catchment lies in India, Jammu and Kashmir (Indian Control), and Pakistan, respectively. In such a complex transboundary river catchment, the global gridded and RS-based datasets can be appropriate alternatives for research purposes [87–89]. Recently, researchers have employed RS and GIS technologies for evaluation of PSE and SY [90]. RS and GIS technologies provide detailed information with a spatiotemporal resolution appropriate for quantifying soil erosion at a

regional/local scale [91,92]. Moreover, use of RS and GIS can reasonably account for the spatiotemporal variability of parameters and catchment heterogeneity [65]. For estimation of water-based erosion, RUSLE coupled with RS and GIS is the most commonly adopted and feasible technique to quantify the magnitude and spatial distribution of soil erosion/loss from rivers' catchments [62,93–97].

A 17 to 27-year study [98] of 9 sediment stations within the Chenab river catchment revealed that there are very high erosion rates. A soil erosion study using the USLE model in similar nearby area also revealed high, very high, and severe soil erosion [99]. Researchers applied the sediment yield index model to the catchment of the Marusudar tributary of the Chenab river, which revealed a high rate of soil erosion [100]. At present, no soil erosion study has been conducted on the complete transboundary Chenab river catchment using the RUSLE model. Keeping in view all the soil erosion issues of the transboundary river catchments, the present study aims to estimate the spatially distributed PSE of the transboundary Chenab river catchment using the RUSLE model integrated with RS and GIS. The spatial distribution of PSE is one of the main targets of this study, so 55 sub-basins were created from the Chenab river catchment. The study also aims to estimate SDR using area, slope, and CN-based approaches, for estimation of sediment yield from the Chenab river catchment. Both PSE and SY were estimated on annual, seasonal, quarterly, and monthly time scales from 1991 to 2020.

2. Material and Methods

2.1. Study Area

The Chenab river catchment is shown in Figure 1. The geographic extent of the Chenab river catchment lies 74°–77.85° E and 32°–34.3° N, while elevation ranges from 240 to 7085 m, and average slope of the river in the catchment is about 25 m/km. It originates in the Kangra and Kulu district of the Himachal Pradesh, India. The Bhaga and Chandra streams emerge from mega snowfields on opposing sides of the Baralcha pass and join the Tandi, Jammu and Kashmir. The climate in the catchment typically comprises two seasons in a year. The Rabi season spans from November to April, the Kharif from May to October. Another climate classification also exists consisting of four seasons, Fall (September, October, November), Winter (December, January, February), Spring (March, April, May), and Summer (June, July, August). The snow-dominant Chenab river catchment [88] receives 65% of precipitation in the monsoon (June, July, August) or pre-monsoon (March, April, May), while 26% precipitation is received in the winter season [101]. The higher altitude of the upper and middle parts of the Chenab river catchment are snow-dominant regions. The mean annual rainfall varies from 278.5 to 2214.9 mm as shown in Figure 2.

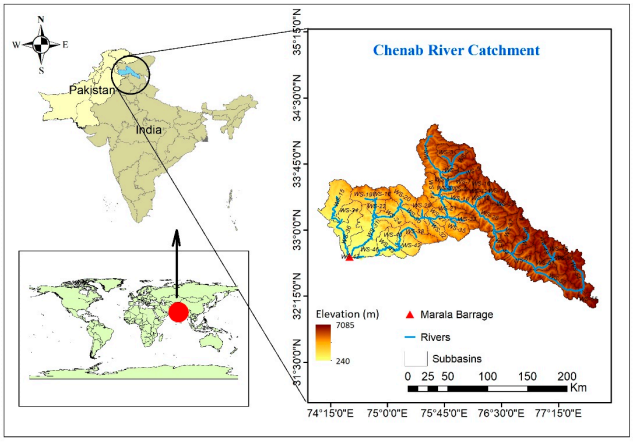

Figure 1. Topographic map of the Chenab River catchment representing river, 55 sub-basins and outlet.

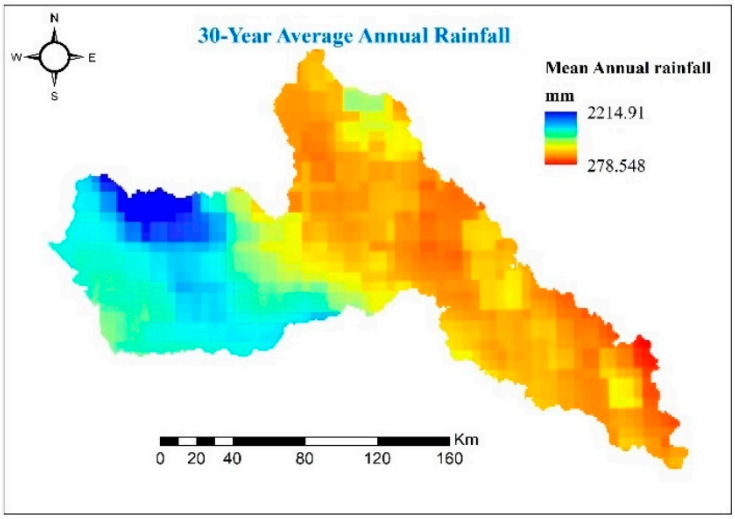

Figure 2. The 30-year average annual rainfall of the Chenab river catchment.

2.2. Methodology

The overall methodology of the research for estimation of PSE and SY is presented in the flowchart (Figure 3). The topographic information, soil data, land use information, and precipitation data were used to estimate all the factors to be used in the RUSLE model for estimation of PSE. The SDRs were estimated based on area, slope and CN approaches, and the SDRs were further used along with PSE to estimate the SY.

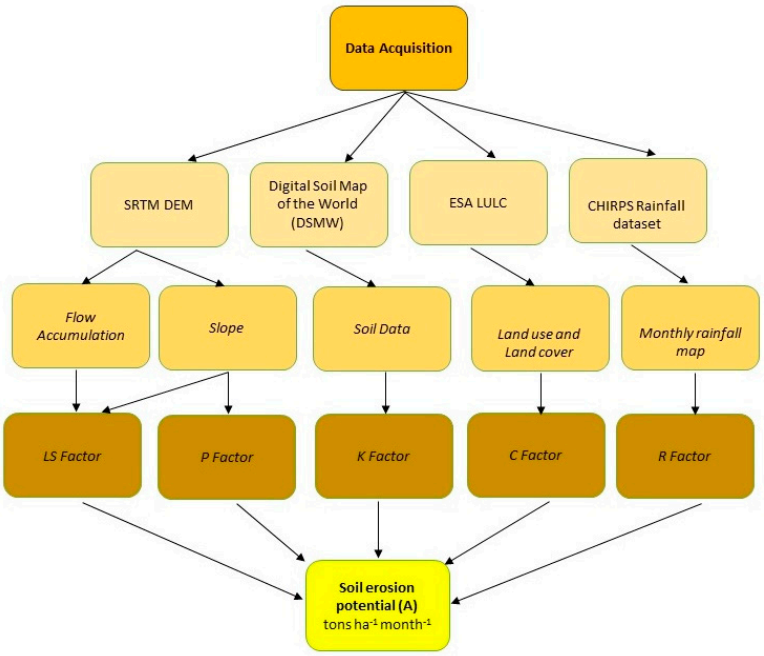

Figure 3. Flow chart for estimation of potential soil erosion and sediment yield.

2.2.1. Datasets Used in the Study

We used the Shuttle Radar Topography Mission Digital Elevation Model (90 m) for watershed delineation, calculation of length and slope factors, and support practice factor based on slope-contour approach. The land use change detection of the river catchment is a major challenge [102] and helps to understand hydrological processes and associated systems of the river basins [103–106]. Due to lack of in situ data, the global land cover map was used at a spatial resolution of 300 m, produced by the ESA Climate Change Initiative

[107]. We estimated land cover management factors using the land use map produced by ESA at a spatial resolution of 300 m. The soil types and texture are also important, along with land use, to understand the hydrological response of the river catchment [108,109]. The Digital Soil Map of the world (DSMW) was used in this study, which is produced by the FAO/ UNESCO. The erosivity factor for 30 years (1991–2020) was estimated using the CHIRPS precipitation data at a spatial resolution of 0.25°.

2.2.2. RUSLE Model for Estimation of Potential Soil Erosion

Wischmeier and Smith developed the USLE for estimation of soil erosion [68]. The new equation (RUSLE) replaces USLE's distinctive rainfall or runoff factor as the rainfall erosivity factor [71]. We used RUSLE to estimate soil erosion at monthly, quarterly, seasonally, and yearly time scales on a surface slope based on the runoff model, soil type, farming practices, topography (slope), and supervision techniques [110]. The RUSLE is an empirical equation that estimates PSE in tons per hectare (Equation (1)).

$$A = R\ x\ K\ x\ L\ x\ S\ x\ C\ x\ P \quad (1)$$

where A is estimated monthly soil erosion (ton ha^{-1} month^{-1}), R is rainfall erosivity factor (MJ mm ha^{-1} h^{-1} month^{-1}), K is soil erodibility factor (t MJ^{-1} ha^{-1} mm^{-1}), L is slope length factor, S is slope steepness factor, C is cover management factor, and P is supporting practices. All these factors of RUSLE were mapped in GIS raster format at quarterly, seasonally, and annual time scales.

Rainfall Runoff Erosivity Factor (R)

Without soil surface protection, the rainfall erosivity factor (R) triggers sheet and rill erosion. Soil loss significantly depends on rainfall because it detaches soil particles from the ground surface and transports them to the river channel [111]. Heavy rainfall events having large droplets size can quickly detach soil particles, compared to droplets of smaller size. The bulk of sheet or rill erosion occurs due to the high runoff generated by a heavy rainfall storm. Rainfall has a significant effect on soil erosion due to the kinetic energy that each raindrop contains, which causes soil particles to detach from the ground surface. We used monthly CHIRPS data for 30 consecutive years (1991–2020) over the Chenab river catchment. In order to estimate the rainfall-runoff erosivity factor of the Chenab river catchment, we calculated R-factor by using Equation (2) developed by Jung et al. [112].

$$R = 0.0378\ x\ X^{1.4190} \quad (2)$$

where R is rainfall runoff erosivity factor (MJ mm ha^{-1} h^{-1} month^{-1}), and X is monthly rainfall amount (mm).

Soil Erodibility Factor (K)

The soil erodibility factor represents the soil's vulnerability to degradation as evaluated under normal unit plot conditions. Soil erodibility is the quantity of soil loss per unit of rainfall erosive energy. We estimated the K factor by using Equation (3) developed by [113]. This depends on soil contents of organic carbon, silt, sand, and clay, obtained from FAO soil data.

$$K = 0.1317.\ f_{csand}.\ f_{cl-si}.\ f_{orge}.\ f_{hisand} \quad (3)$$

$$f_{csand} = \ (0.2 + 0.3 \exp[\ -0.256\ x\ ms\ x \left(1 - \frac{msilt}{100}\right)]) \quad (4)$$

$$f_{cl-si} = \ (\frac{msilt}{mc + msilt})^{0.3} \quad (5)$$

$$f_{orge} = (1 - \frac{0.0256\ x\ orgC}{orgC + exp[3.72\ - 2.95\ x\ orgC]}) \quad (6)$$

$$f_{hisand}\ (\ 1 - \frac{0.7\ x\left(1 - \frac{ms}{100}\right)}{\left(1 - \frac{ms}{100}\right) + exp\left[-5.51 + 22.9\left(1 - \frac{ms}{100}\right)\right]}) \quad (7)$$

where ms is % sand content in topsoil, msilt is % silt content in topsoil, mc is % clay content in top soil, and orgC is % organic carbon content in top soil. We estimated the K factor by Equation (3). A maximum of four soil types were identified in the soil map using the FAO soil data. The soil erodibility factor was estimated based on the sand, silt, and clay percentages.

Slope-Length and Slope-Steepness Factor (LS)

The LS factor represents the effects of topography on soil erosion by including slope-length factor (L) and slope-steepness factor (S), both of which influence overland flow velocity [114]. The Topographic slope-length (L) and slope-steepness (S) reflect a ratio of soil erosion under defined conditions compared to soil loss at a site with a "normal" slope steepness of 9% and a slope length of 22.6 m [62]. Because the LS-factor causes high runoff velocity and hence more runoff volume, the highest slope has the greatest danger of soil erosion. The equation of LS is given as;

$$LS\ (\frac{\lambda}{22.13})^m\ x\ (\frac{sin\ \beta}{0.0896})^n \quad (8)$$

$$\beta = \frac{sin\ \theta\ /0.0896}{3\ x\ sin\ \theta^{0.8} + 0.56} \quad (9)$$

where θ is Slope of watershed (degree), n is 1.3

λ = slope-length (m) = flow acc. x cell size

m = variable slope length exponent = $\frac{\beta}{1+\beta}$

Cover Management Factor (C)

The dimensionless cover and management factor plays its role in reducing soil erosion, and depends on the land use patterns of the area [115]. The C factor is the ratio between soil loss from areas with protective cover and management to soil loss from continuously clean tilled fallow land [116]. The C factor varies from 0 to 1 depending on land use characteristics, excluding water bodies [117].

Supporting Conservation Practice Factor (P)

The P-factor is the ratio of soil loss induced by each type of conservation technique to the comparable erosion generated by uphill and downhill sloped cropping [110,118]. It modifies the volume and water discharge, hence affecting the magnitude of soil erosion. The support conservation techniques used in the catchment, such as contouring, terracing, strip cropping, etc., are referred to as the support practice factor. The P factor has a value between 0 and 1, with 0 representing very good preservation practice, and one indicating no preservation technique [45].

2.2.3. Estimation of Sediment Yield

$$SY = SDR\ x\ A \quad (10)$$

where SY is in tons/month, SDR (fraction), and A is PSE (tons/month).

Estimation of Sediment Delivery Ratio

The SDR is the ratio of sediments delivered at outlet to the gross erosion of the catchment upstream of the measurement location [119], and SDR represents several processes which are involved in estimation of SY [120]. Although the United States Department of Agriculture has published a handbook [121] in which the SDR is linked to drainage areas, there is no perfect process for estimating SDR. A variety of factors can influence SDR, including sediment load, texture, proximity to the mainstream, channel density, basin area, slope, length, land use, rainfall, and runoff. The Soil Conservation Service (SCS) curve is the established relationship between SDR and drainage area. For example, a watershed with a higher channel density has a higher SDR than a catchment with a lower channel density. The SDR of a watershed with steep slopes is greater than that of a watershed with flat and large valleys. The size of the area of interest should also be defined in order to predict SDR. The higher the area size, the smaller the fraction of SDR since large areas have more chance of trapping soil particles. The SDR equations have been derived by several researchers in different river basins of the world [122–125]. The researchers correlated the SDR with area [121] and developed their equation as follows:

$$SDR = 0.5656\, x\, A^{-0.11} \quad (11)$$

where A is the area of watershed in sq. miles (mi²).

The researchers [126] also correlated the *SDR* with the slope and developed the equation as follows:

$$SDR = 0.627\, x\, S^{0.403} \quad (12)$$

where S is the slope of watershed in degree.

The relief-length ratio is prepared by getting the maximum and minimum value of the elevation of the catchment, then by taking the difference of maximum and minimum elevation and finally dividing it by the length of the river. SDR against CN is prepared according to the empirical equation. According to the research [74], the SDR is related to watershed area, relief-length ratio, and SCS CN, and the following equation was derived in a study conducted on 15 Texas basins:

$$SDR = 1.366\, x\, 10^{-11}\, x\, A^{-0.0998}\, x\, ZL^{0.3629}\, x\, CN^{5.444} \quad (13)$$

where A is the area in km² and ZL is the relief-length ratio in m/km

The hydrologic soil group and ground cover are used to calculate the CN. In general, the most reliable findings are achieved when each sub-catchment is homogeneous, with as few CNs as possible. When a large number of CNs are averaged into a single sub-catchment, the results are not necessarily the same as when multiple sub-catchments are produced and combined together. A single sub-catchment, for example, will only have one peak; however, merging many sub-catchments might result in a multi-peak hydrograph.

3. Results

3.1. Factors of the RUSLE Model

The 30-year average rainfall erosivity factor maps at annual, seasonal (rabi, kharif), and quarterly time scales (fall, winter, spring, and summer) are presented in Figure 4.

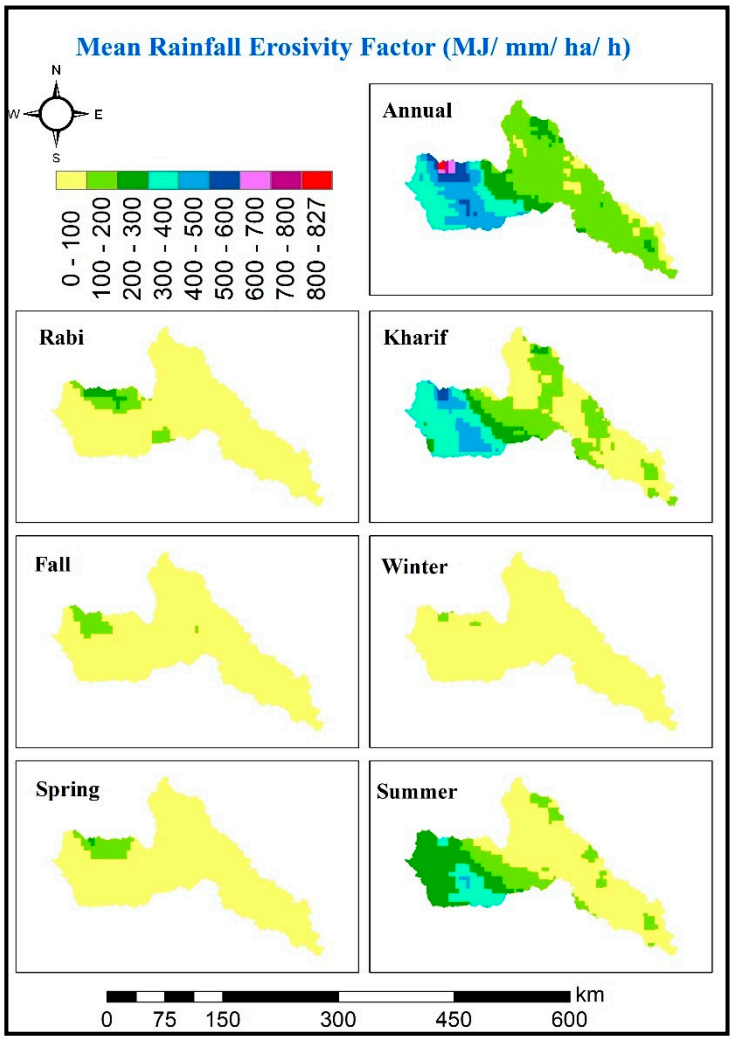

Figure 4. 30-year average annual, seasonal, and quarterly rainfall erosivity factors for the Chenab river catchment.

The peak rainfall erosivity factor was 826.8, 277.9, 558.5, 199, 115.3, 217.7, and 426.8 MJ mm^{-1} ha^{-1} h^{-1} for annual, rabi, kharif, fall, winter, spring, and summer, respectively. The spatial distribution of all the maps in Figure 4 reveals that the upper parts of the catchment have lower rainfall erosivity, and the lower parts of the catchment have very high erosivity because of high rainfall over the lower part as shown in Figure 2. Higher rainfall erosivity has been observed in kharif season (May to October), and in summer season. The maps of rabi season (November to April), fall, winter and spring seasons reveal that higher erosivity has been observed in higher latitudes in the lower parts of the catchments.

The estimated soil erodibility factor values using %sand, %silt, %clay, and % OC are given in Table 1. The four soil types were found in the river catchment, and K value ranges from 0.0174 to 0.023.

Table 1. Soil erodibility factor value calculated for soil type in the Chenab river catchment.

Soil Unit Symbol	% Sand Topsoil	% Silt Topsoil	% Clay Topsoil	% OC Topsoil	K Factor Value
I	58.9	16.2	24.9	0.97	0.0196588
Be	36.4	37.2	26.4	1.07	0.0223028
Lo	76	9.9	14.1	0.41	0.0174135
Jc	39.6	39.9	20.6	0.65	0.0232663

The 30-year average soil erodibility, slope-length and slope-steepness, cover management, and supporting conservation practice factors map of the Chenab river catchment is presented in Figure 5. The map of K factor reveals that most of the catchment is below 0.0197, while some portions of the catchment are in areas of high soil erodibility (greater than 0.0197).

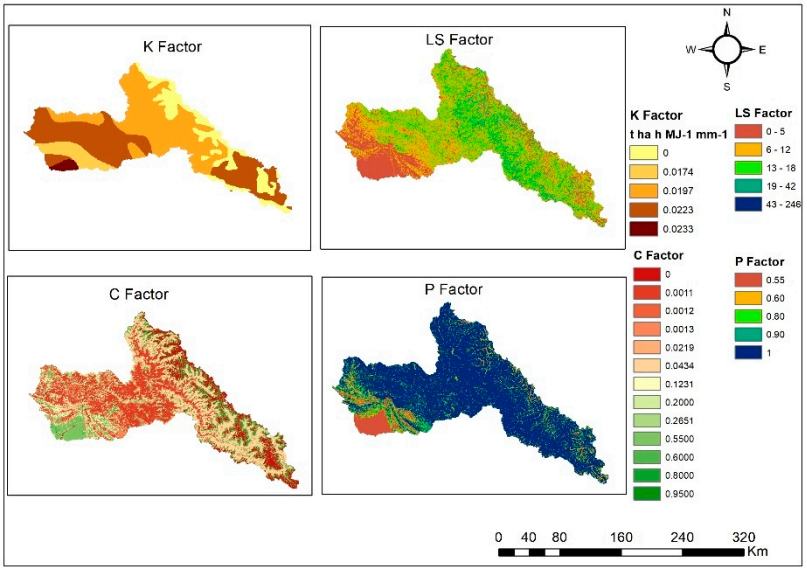

Figure 5. Soil erodibility, slope-length and slope-steepness, cover management, and supporting conservation practice factors in the Chenab river catchment.

The LS factor map of the Chenab river catchment is presented in Figure 5, which reveals that most of the catchment lies under two main classes, 0 to 5 in upper and middle parts of the catchment, and 13 to 18 in lower parts of the catchment. Therefore, the effect of LS on the PSE is not higher, as a higher LS factor area is not common in the catchment. The land use map of Chenab river catchment prepared using land use data of ESA is presented in Figure 6. The upper parts of the river catchment are covered with snow, consolidated bare land, grassland, and mosaic trees and shrubs. The middle to lower parts of the catchment are covered with tree cover and mosaic cropland, while the lowest parts of the catchment near to the outlet are covered with irrigated cropland. The cover management factor values were estimated (Table 2) using the land use information of ESA.

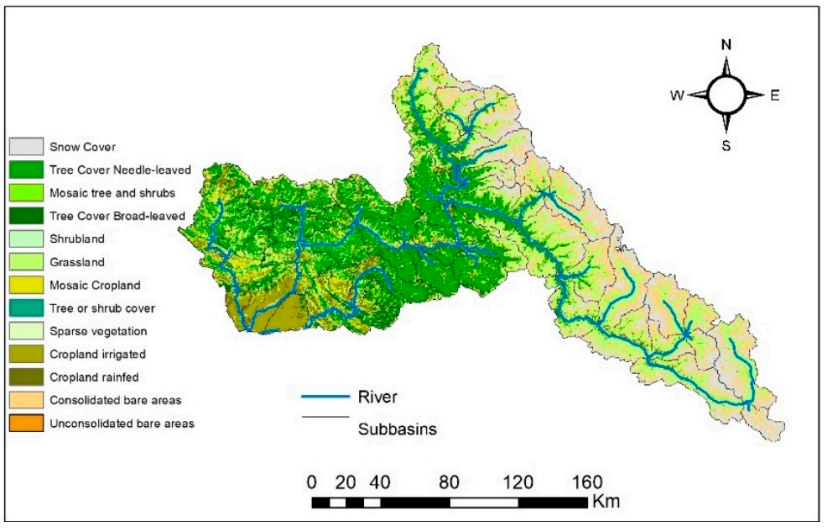

Figure 6. Land use of the Chenab river catchment developed using European Space Agency land use.

Table 2. Cover management factor values of the Chenab river catchment.

Land Use and Land Cover Class	C Factor Value	Source
Snow Cover	0	[127]
Tree Cover Needle-leaved	0.0011	[127]
Mosaic tree and shrubs	0.0012	[127]
Tree Cover Broad-leaved	0.0013	[127]
Shrub land	0.0219	[127]
Grassland	0.0434	[127]
Mosaic Cropland	0.1231	[127]
Tree or shrub cover	0.2000	[127]
Sparse vegetation	0.2651	[127]
Cropland irrigated	0.5500	[127]
Cropland rainfed	0.6000	[127]
Consolidated bare areas	0.8000	[127]
Unconsolidated bare areas	0.9000	[127]

The cover management factor map was developed based on the C value of various vegetative coverings, as illustrated in Figure 5. The snow-covered areas of the upper catchment are under the lowest C values, while the bare areas in of the upper catchment are under high C values, while most of the upper to middle parts of the catchment are under medium C value (0.0434 to 0.1232). The middle to lower parts of the catchment are under lower C values, and the extreme lower parts of the catchment are under slightly higher C values.

In this research, data from the literature [128] was obtained for estimation of conservation management factor against % slope as presented in Table 3. As in situ crop information cannot be obtained, the average of the conservation practices was used in order to estimate the P value to be used in RUSLE. The P factor map for the Chenab river catchment is presented in Figure 5. Most of the catchment is under a high value of P, while the catchment areas near to the outlet are under lower values of P.

Table 3. Conservation management factor values for contouring, strip cropping, and terracing against slope.

Slope (%)	Contouring	Strip Cropping	Terracing
0.0–7.0	0.550	0.270	0.100
7.0–11.3	0.600	0.300	0.120
11.3–17.6	0.800	0.400	0.160
17.6–26.8	0.900	0.450	0.180
26.8 >	1.000	0.500	0.200

3.2. Potential Soil Erosion

The 30-year annual average PSE from the Chenab river catchment is presented in Figure 7. The 30-year average PSE from the Chenab river catchment was estimated as 177.8, 61.5, 310.3, 39.5, 26.9, 47.1, and 99.1 tons/ha for annual, rabi, kharif, fall, winter, spring, and summer time scales, respectively. The minimum values of PSE are on the snow cover areas, and lower values are seen also on tree cover and irrigated croplands. The bare areas near the rivers and the upper latitudes of the lower parts of the catchments are under medium PSE. On an annual time-scale, there is less area of catchment which has more than 10 PSE. The kharif season shows higher PSE values compared to the rabi season, mainly due to heavy precipitation in monsoon season and high magnitude of runoff due to rainfall-runoff and snowmelt. The PSE in summer season is higher in different areas of the catchment as compared to the fall, winter, and spring seasons.

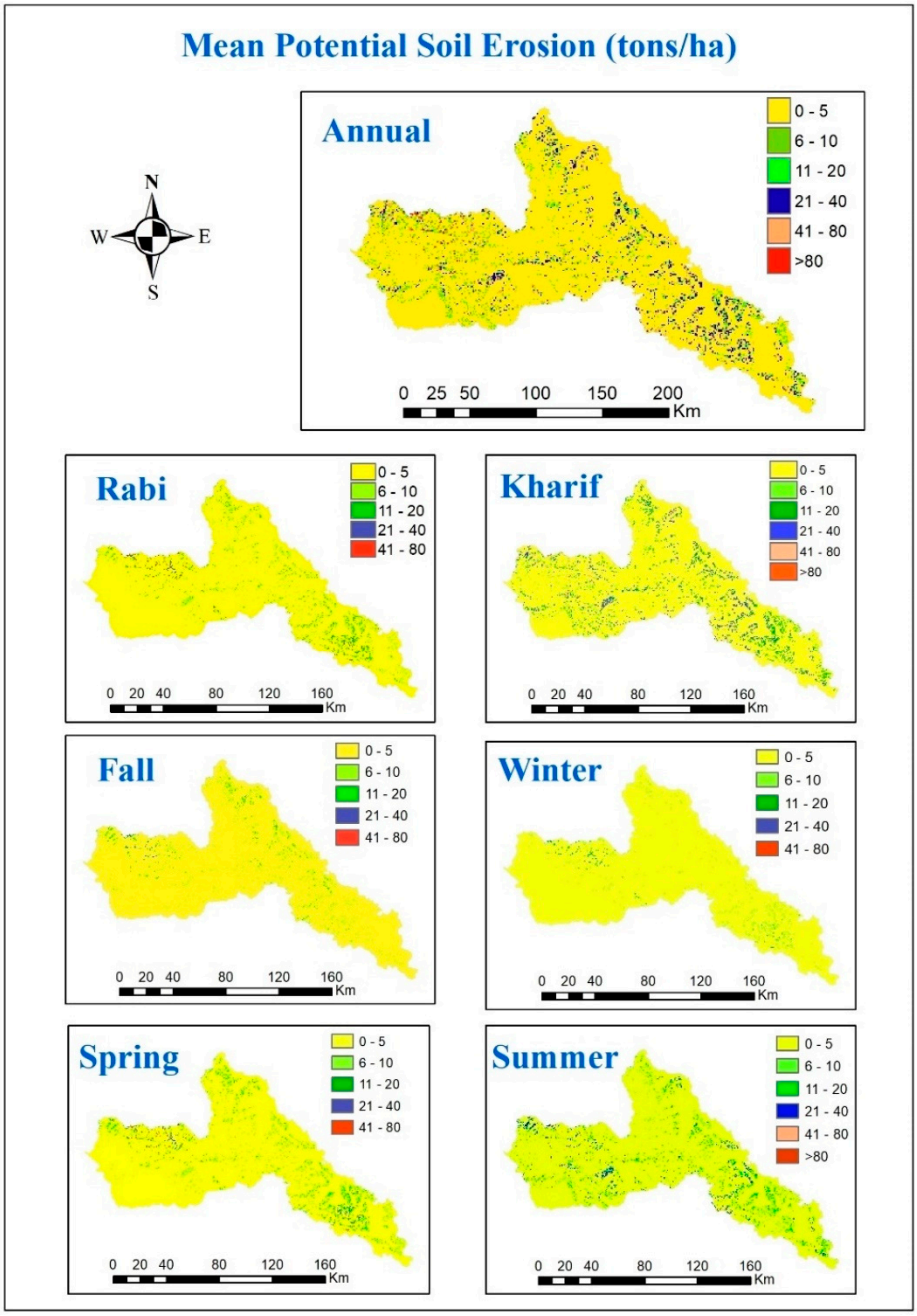

Figure 7. 30-year average potential soil erosion from the Chenab river catchment at different time-scales.

The PSE distribution for all the mentioned time-scales is grouped into six soil erosion intensity classes (slight, moderate, high, very high, severe, and very severe) as per the literature [129] as shown in Figure 8.

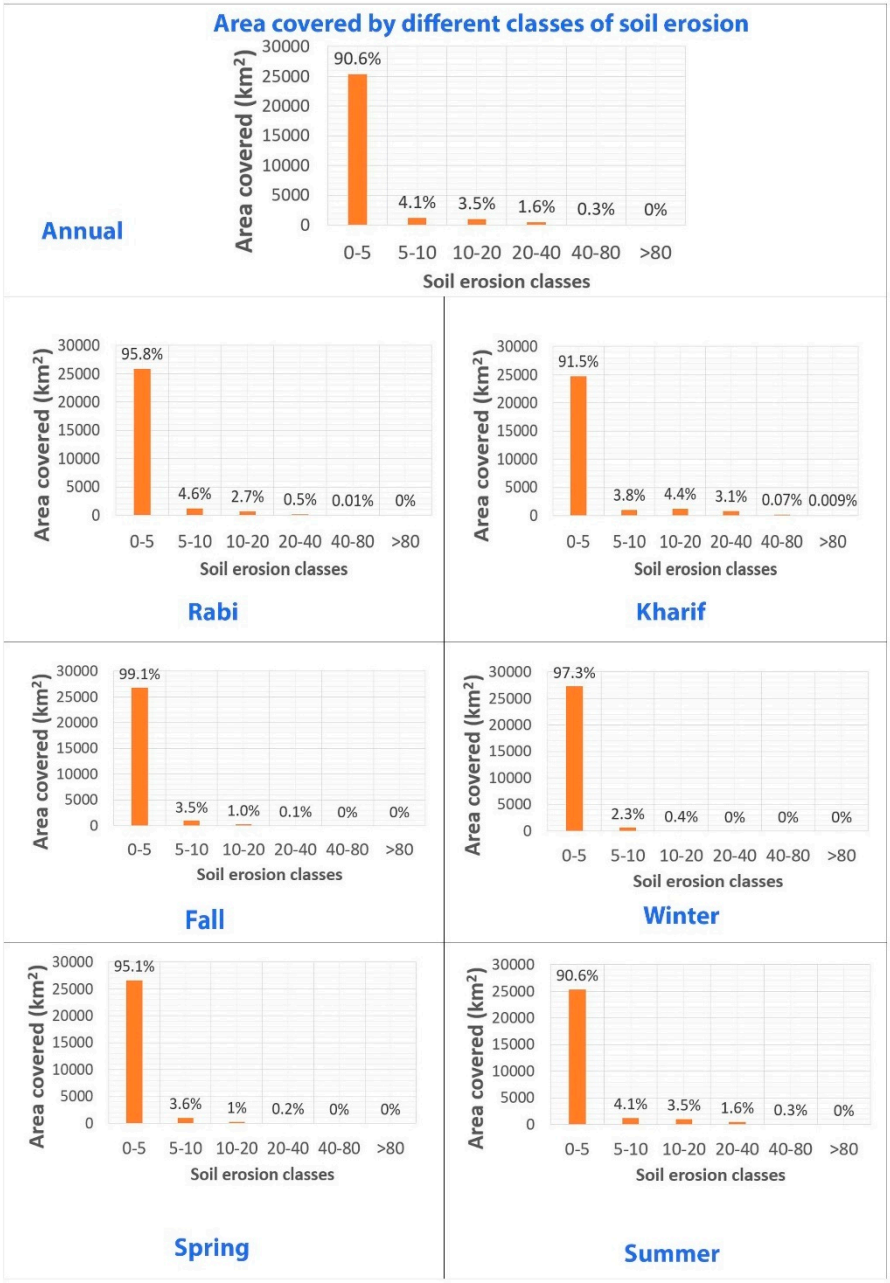

Figure 8. Catchment area percentage under different soil erosion classes based on PSE (ton/ha).

These six classes have value ranges from 0–5, 5–10, 10–20, 20–40, 40–80, and >80 tons/ha, respectively. On an annual time-scale, most PSE is under slight intensity, while areas are also under moderate, high, and very high, but the percentage of area in these three intensity classes is less. In the kharif season, there is more area in high and very high intensity classes as compared to the rabi season. In the summer season, there is area under very high intensity of erosion as compared to fall, winter, and spring season. It is obvious from Figure 8 that the percentage of area in 0–5 class is more than 90% for all the time periods.

3.3. Sediment Yield

The SY from the Chenab river catchment was estimated using area, slope, and CN-based approaches. The CN for the Chenab river catchment is presented in Figure 9. The CN values in the snow-covered areas and some lower parts of the Chenab river catchment are higher, the central parts of the catchment are under medium CN values, and some

lower parts of the catchment are under low CN values. The sub-catchment-wise SDR based area, slope, and CN are presented in Figure 10. There is reliable agreement between the SDRs based on area and slope, while the slope-based SDR is higher than the other. The CN-based SDR was higher than the others, while the higher CN-based SDR values were observed in sub-catchment numbers 10, 11, 12, 23, and 47.

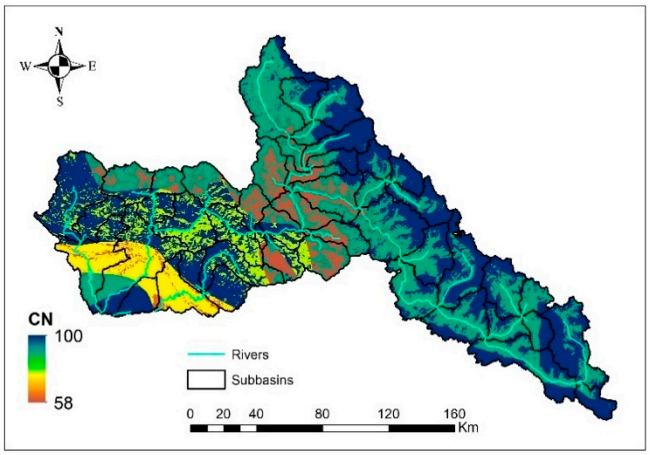

Figure 9. CN map of the Chenab river catchment.

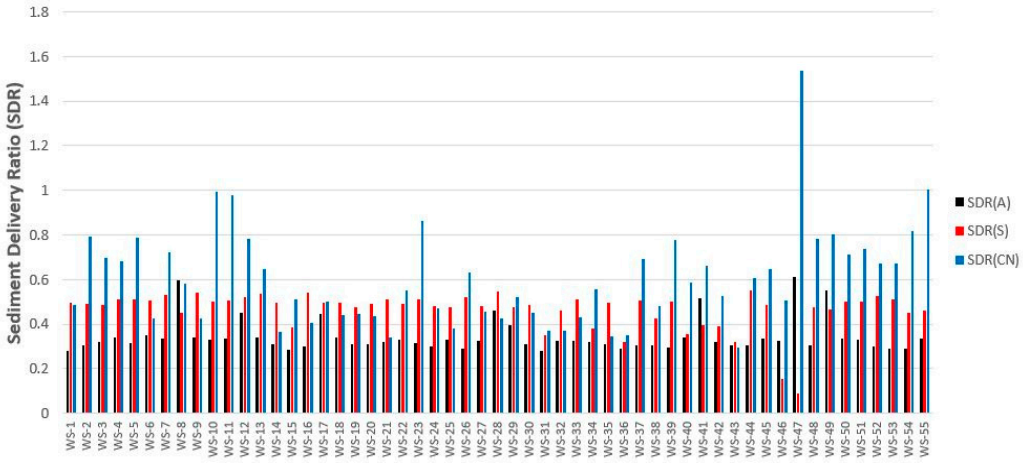

Figure 10. Mean Sediment delivery ratio in each micro-catchment.

In the area-based SDR, watershed (WS)-47 exhibited the highest SDR of 0.61 having a 0.5 sq. mile area, which contributes 0.0045% of the total area of the catchment, while the WS-1 had the minimum SDR of 0.281 consisting of 565.8 sq. miles area which contributes 5.2% of the total area of the catchment/watershed. In the slope-based SDR, the WS-44 exhibited the highest SDR of 0.551 having a 270.118 sq. miles area which contributes 2.48% of the total area of the watershed, while the WS-47 had the minimum SDR of 0.08 consisting of a 0.5 sq. mile area which contributes 0.0045% of the total area of the watershed. In the CN-based SDR, the overall ratio seemed high as compared to area and slope module, in which WS-47 contributed the highest SDR of 1.53 having a 0.5 sq. mile area which contributes 0.0045% of the total area of the watershed. On the other hand, the WS-43 had the minimum SDR consisting of 265.98 sq. miles area which contributes 2.44% of the total area of the watershed.

The annual sediment yield pattern over the last 30 years is presented in Figure 11. A similar pattern among area, slope, and CN-based annual SY has been observed. The highest SY was observed in 2014, and it showed that the sediment load was highest due to intense precipitation and surface runoff. In 2014, the area, slope and C-based SY was observed as 7,886,149, 12,032,723, and 14,550,254 tons, respectively. However, in 1998, the

SY had the lowest value of 1,183,469, 1,733,782, and 2,067,188 tons based on area, slope and CN, respectively. The time series trends analysis of SY indicated an increase of 0.0895, 0.1387, and 0.1698 million tons per year for area, slope, and CN-based approaches, respectively.

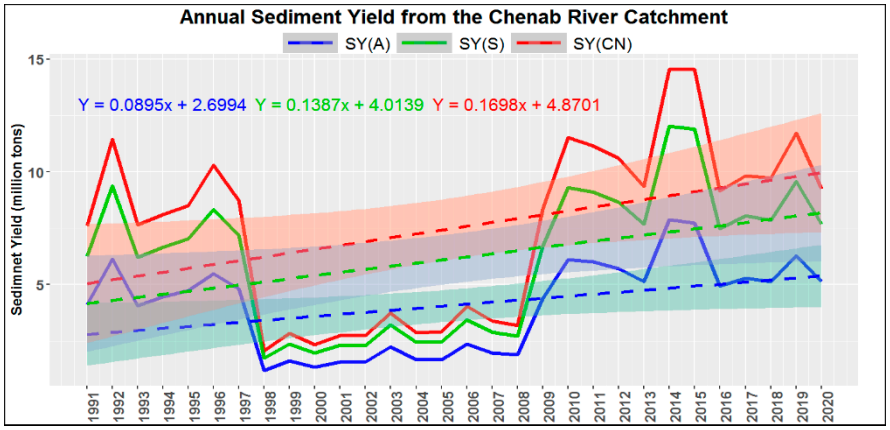

Figure 11. Annual sediment yield from the Chenab river catchment 1991 to 2020.

The SY over the last 30-year in Rabi and Kharif season is presented in Figure 12.

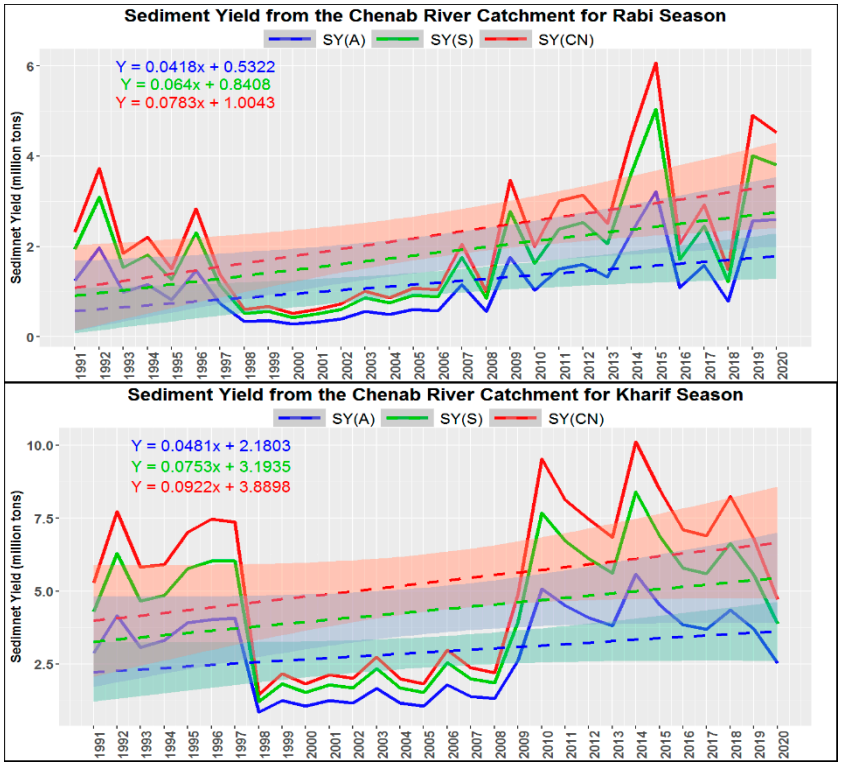

Figure 12. Sediment yield from the Chenab river catchment for rabi and kharif seasons from 1991–2020.

The overall contribution of the kharif season was higher than that of the rabi season. In 2014, the highest SY of the kharif season based on area, slope, and CN was 5,574,869, 8,405,752, and 10,124,635 tons, respectively. In 2015, the highest SY of the rabi season based on area, slope, and CN was 3,264,869, 5,015,752, and 8,104,635 tons, respectively. The SY time series trends analysis of the rabi season indicated an increase of 0.0418, 0.064, and 0.0783 million tons per year for area, slope, and CN-based approaches, respectively. The SY time series trends analysis of the kharif season indicated an increase of 0.0481,

0.0753, and 0.0922 million tons per year for area, slope, and CN-based approaches, respectively.

The SY for fall, winter, spring, and summer is presented in Figure 13.

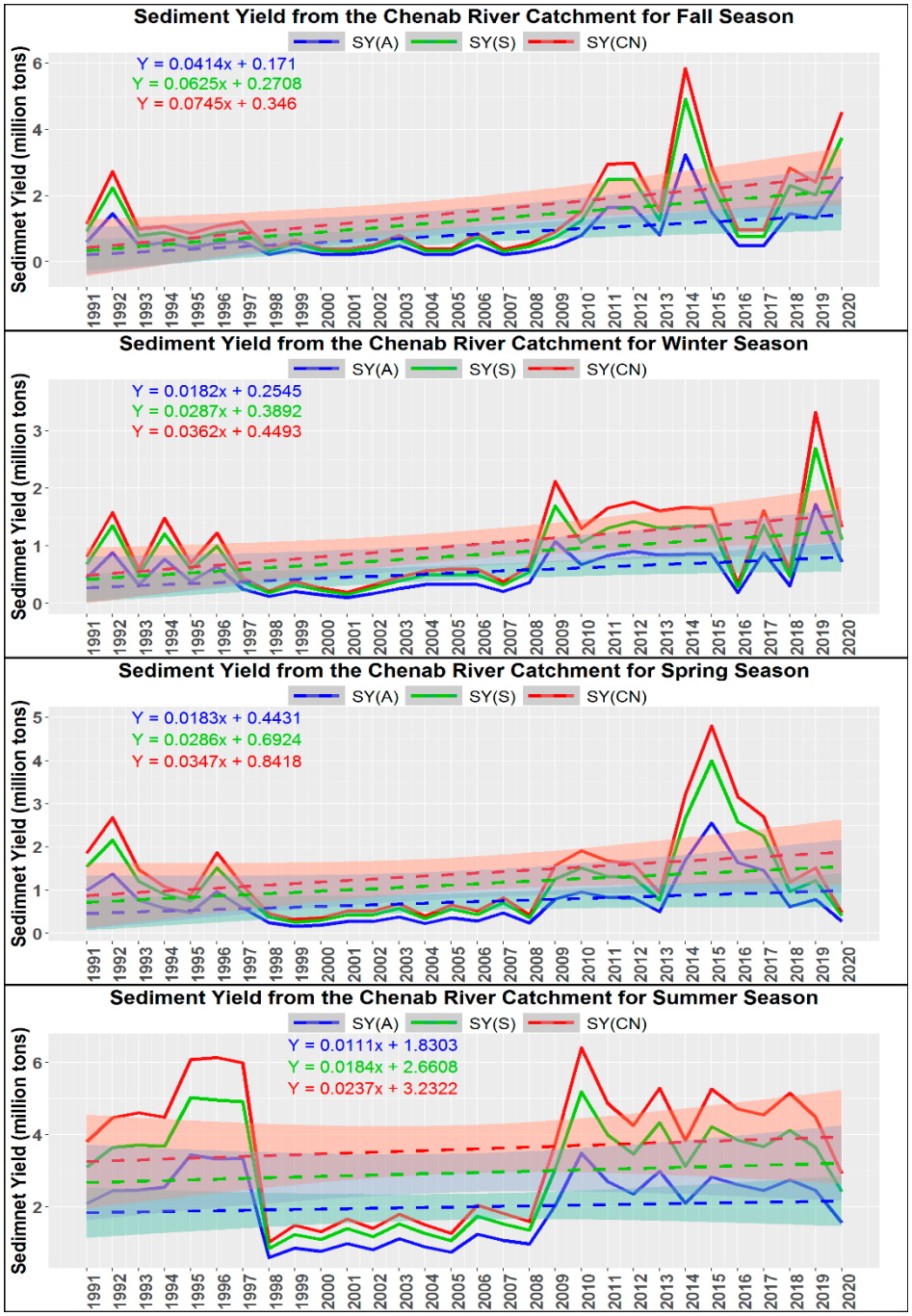

Figure 13. Sediment yield from the Chenab river catchment for fall, winter, spring, and summer seasons from 1991–2020.

The SY for fall period was higher in 1992, 2010, 2011, 2012, 2014, 2018, 2019, and 2020. The SY for winter period was higher in 1992, 1994, 1996, 2008–2014, 2017, 2019, and 2020. The SY for spring period was higher in 1991–1993, 1996, 2009–2012, 2014–2017. The SY for the summer season was higher in 1991–1997 and 2009–2020.

The monthly sediment yield for the last 30 years is presented in Figure 14. The highest SY values of 3,125,536 tons, 4,745,077 tons, and 5,643,741 tons for area, slope, and CN, respectively, were observed in September 2014. Similarly, the lowest values of 11,484 tons,

17,904, and 21,811 tons for area, slope, and CN, respectively, were observed in November 1998. The time series trends analysis of SY indicated an increase of 0.0006, 0.001, and 0.0012 million tons per month for area, slope, and CN-based approaches, respectively.

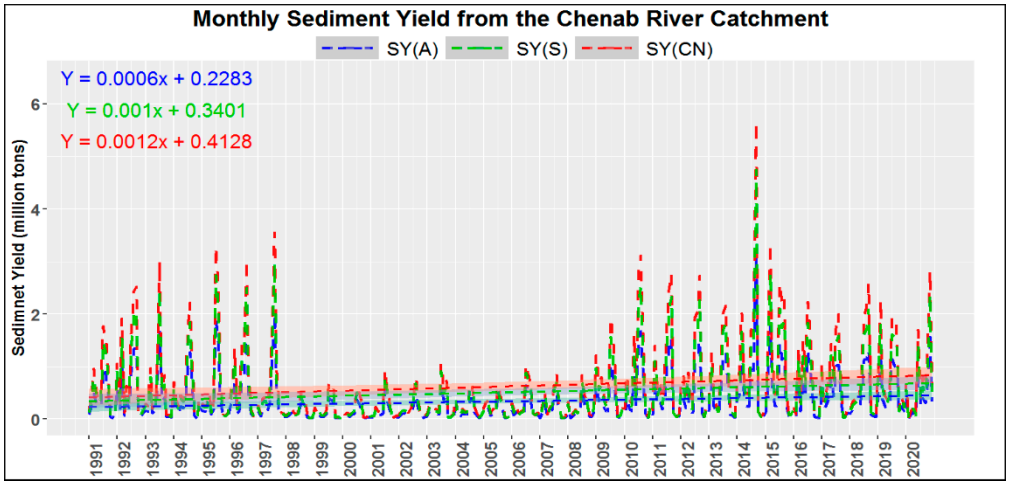

Figure 14. Monthly sediment yield from the Chenab river catchment from 1991 to 2020.

4. Discussion

Soil erosion is a severe issue, particularly in the Chenab river catchment, where various variables contribute to fast soil erosion and sedimentation. The rate of runoff and sedimentation is accelerated by factors such as the region's steep slope, temperature, velocity of flowing water, and environmental conditions [130]. The impact of a raindrop on the soil surface and the cutting force of running water causes soil particles to detach. Raindrop splash, despite having a minimal effect, triggers downslope transport of eroded soil particles [131]. High intensity rainfall makes the detachment of soil particles quicker and causes the mass movement of sediments along the runoff generated. Early in the rainy season, when the rainfall is intense but the vegetation has not developed enough to protect the soil, is the most favorable time for erosion. In general, the time between plowing and crop emergence is referred to as the farmer's interval [132]. The CHIRPS precipitation data was incorporated in this research as it has better performance over areas that usually receive high rainfall [133].

Slope also varies, decrease in slope causing velocity to decrease, and ultimately to sediment transport decreases [134], which further increases the rate of sediment deposition. The topography and high elevation are usually the main reason for high intensity precipitation [135]. The K factor of the study area varied from 0.019 to 0.023. The soil, having low moisture content and permeability, represents a low K factor value. Soil erosion is closely concerned with the state of land use and agriculture practices, and cover management, as most of the Chenab river catchment was under 0 to 5 tons ha^{-1}. The annual average PSE rates throughout the world are estimated as 12 to 15 tons ha^{-1}, while the river catchment areas with a PSE of lower than 3 tons ha^{-1} $year^{-1}$ are generally below the estimated tolerable soil loss level and should be exempt from any mitigating activities.

Though different soil erosion studies have been carried out on the Chenab river catchment with various models and techniques, this is the first time that estimation of PSE and SY for the last 30 years has been performed using the RUSLE model and SDRs on annual, seasonal, quarterly and monthly time-scales The SDR is estimated using area, slope, and CN-based approaches, and slope-based estimations are being applied by researchers around the world [136–144]. It is also observed in the study that SDR decreased with increase in area or stream length, and this is also observed by other researchers [124,145]. Moreover, topography-based SDR (slope) is scale dependent, and the scale dependency of such SDR has also been observed by researchers [146–148]. The RUSLE and

SDR (mainly slope-based) are being applied by the scientific community for estimation of PSE and SY [149–155]. The RUSLE is used at multiple spatial scales by dividing a pixel into sub-regions with similar features and linking them to a GIS data structure [110]. Such models are now commonly in use to create an environment-based information system that allows for the estimation and evaluation of various management scenarios [156]. This methodology, however, has certain limitations but provides reliable results by identifying the high PSE areas. The RUSLE model was selected and applied to nearby similar rivers' catchments [97,135,157].

The complete lower parts of the catchments are under high rainfall erosivity, therefore soil and water conservation measures and crop management practices are needed in order to reduce the rainfall erosivity, which will ultimately reduce the overall PSE and SY. The organic content of the soil reduces soil erodibility because increase in organic matter reduces the susceptibility of soil detachment, and increases infiltration, which further reduce runoff and thus soil erosion. The organic content should be increased in high K values areas by incorporating manure. With the novelty of providing soil loss estimates at finer spatial and temporal scales, the findings of this study can be useful for assessing soil erosion in other data-scarce areas, and can be helpful to resource conservation experts for making informed decisions.

5. Conclusions

The following conclusions have been derived from a 30-year study of soil erosion from the Chenab river catchment using RUSLE and SDR approaches;

- The analysis results depicted that the range of average annual PSE was from 0.0 to 177.8 tons/ha, while, in the Rabi and Kharif season, the range of average PSE was between 0.0 to 61.5 tons/ha and 0.0 to 310.2 tons/ha. Similarly, in Fall, Winter, Spring, and Summer timescales, the range of average PSE was from 0 to 39.5, 26.9, 47.1, and 99.1 tons/ha, respectively.
- The time series trends analysis of SY indicated an increase of 0.0895, 0.1387, and 0.1698 million tons per year for area, slope, and CN-based approaches, respectively.
- The annual SY estimated by area, slope and CN was highest in 2014 with 7,886,149, 12,032,723, and 14,550,254 tons, respectively. The average PSE of Kharif season was highest (70%), followed by Fall (41%), Rabi (30%), Summer (26%), Spring (22%), and Winter (11%) season.
- The annual SY estimated by area, slope and CN was minimum in 1998 with 1,183,469, 1,733,728, and 2,067,188, respectively. The average PSE of Kharif season was highest for soil loss (71%), followed by Summer (49.5%), Rabi (29%), Spring (22%), Fall (18%), and Winter (10.5%), respectively.
- Inter-comparison of SY estimated by SDR based on slope and CN showed the consistency pattern and thus proved the authenticity of empirical models, but the SY estimated by area-based SDR was less compared to the slope and CN-based SDR Approaches.

Author Contributions: Conceptualization, M.G.A., R.H.A. and S.A.; Methodology, M.G.A., A.N. and S.A.; Software, R.H.A. and M.M.W.; Formal Analysis, A.N., M.W. and R.A.A.; Investigation, M.M.W., R.A.A. and M.J.M.C.; Resources, M.G.A., M.J.M.C. and S.A.; Data Curation, A.N., M.W. and M.K.L.; Writing—Original Draft Preparation, M.G.A., A.N. and I.S.; Writing—Review & Editing, S.A., M.J.M.C. and I.S.; Visualization, M.G.A., I.S. and M.K.L.; Supervision, A.N. and R.H.A. All authors have read and agreed to the published version of the manuscript.

Funding: This research has not received any external funding.

Institutional Review Board Statement: Not applicable.

Data Availability Statement: Data belongs to the authors.

Conflicts of Interest: The authors declare no conflict of interest.

References

1. Bini, C. Soil: A precious natural resource. In *Conservation of Natural Resources*; Kudrow, N.J., Ed.; Nova Science Publishers: Hauppauge, NY, USA, 2009, pp. 1–48.
2. Pimentel, D.; Kounang, N. Ecology of Soil Erosion in Ecosystems. *Ecosystems* **1998**, *1*, 416–426, https://doi.org/10.1007/s100219900035.
3. Zhao, G.; Mu, X.; Wen, Z.; Wang, F.; Gao, P. Soil erosion, conservation, and eco-environment changes in the Loess Plateau of China. *Land Degrad. Dev.* **2013**, *24*, 499–510, https://doi.org/10.1002/ldr.2246.
4. Costanza, R.; d'Arge, R.; De Groot, R.; Farber, S.; Grasso, M.; Hannon, B.; Limburg, K.; Naeem, S.; O'neill, R.V.; Paruelo, J. The value of the world's ecosystem services and natural capital. *Nature* **1997**, *387*, 253–260, https://doi.org/10.1038/387253a0.
5. Swinton, S.M.; Lupi, F.; Robertson, G.; Hamilton, S.K. Ecosystem services and agriculture: Cultivating agricultural ecosystems for diverse benefits. *Ecol. Econ*. **2007**, *64*, 245–252, https://doi.org/10.1016/j.ecolecon.2007.09.020.
6. Alewell, C.; Borrelli, P.; Meusburger, K.; Panagos, P. Using the USLE: Chances, challenges and limitations of soil erosion modelling. *Int. Soil Water Conserv. Res.* **2019**, *7*, 203–225, https://doi.org/10.1016/j.iswcr.2019.05.004.
7. Amundson, R.; Berhe, A.A.; Hopmans, J.W.; Olson, C.; Sztein, A.E.; Sparks, D.L. Soil and human security in the 21st century. *Science* **2015**, *348*, 1261071, doi:10.1126/science.1261071.
8. Veerasingam, S.; Venkatachalapathy, R.; Ramkumar, T. Heavy metals and ecological risk assessment in marine sediments of Chennai, India. *Carpathian J. Earth Environ. Sci.* **2012**, *7*, 111–124.
9. Tosic, R.; Dragicevic, S.; Kostadinov, S.; Dragovic, N. Assessment of Soil Erosion Potential by the Usle Method: Case Study, Republic of Srpska—BiH. *Fresenius Environ. Bull.* **2011**, *20*, 1910–1917.
10. Dotterweich, M. The history of soil erosion and fluvial deposits in small catchments of central Europe: Deciphering the long-term interaction between humans and the environment—A review. *Geomorphology* **2008**, *101*, 192–208, https://doi.org/10.1016/j.geomorph.2008.05.023.
11. Yang, D.; Kanae, S.; Oki, T.; Koike, T.; Musiake, K. Global potential soil erosion with reference to land use and climate changes. *Hydrol. Process.* **2003**, *17*, 2913–2928, https://doi.org/10.1002/hyp.1441.
12. Routschek, A.; Schmidt, J.; Kreienkamp, F. Impact of climate change on soil erosion—a high-resolution projection on catchment scale until 2100 in Saxony/Germany. *Catena* **2014**, *121*, 99–109, https://doi.org/10.1016/j.catena.2014.04.019.
13. Lal, R. Soil degradation by erosion. *Land Degrad. Dev.* **2001**, *12*, 519–539, https://doi.org/10.1002/ldr.472.
14. Lal, R. Soil Erosion by Wind and Water: Problems and Prospects. In *Soil Erosion Research Methods*; Routledge: London, UK, 2017; pp. 1–10, https://doi.org/10.1201/9780203739358-1.
15. Pimentel, D. Soil Erosion: A Food and Environmental Threat. *Environ. Dev. Sustain.* **2006**, *8*, 119–137, https://doi.org/10.1007/s10668-005-1262-8.
16. Bhattarai, R.; Dutta, D. Estimation of Soil Erosion and Sediment Yield Using GIS at Catchment Scale. *Water Resour. Manag.* **2006**, *21*, 1635–1647, https://doi.org/10.1007/s11269-006-9118-z.
17. Rojas-González, A.M. Soil erosion calculation using remote sensing and GIS in RÍO grande de Arecibo Watershed, Puerto Rico. In Proceedings of the ASPRS 2008 Annual Conference Bridging the Horizons: New Frontiers in Geospatial Collaboration, Portland, OR, USA, 28 April–2 May 2008.
18. Marsh, W.M.; Grossa, J., Jr. *Environmental Geography: Science, Land Use, and Earth Systems*; John Wiley and Sons: Hoboken, NJ, USA, 1996.
19. Wang, M.; Pan, J.; Zhao, J. Quantitative survey of the soil erosion change based on GIS and RS: Take the Qingcheng area as an example. *Agric. Res. Arid. Areas* **2007**, *25*, 116–121.
20. Nyakatawa, E.; Reddy, K.; Sistani, K. Tillage, cover cropping, and poultry litter effects on selected soil chemical properties. *Soil Tillage Res.* **2001**, *58*, 69–79, http://dx.doi.org/10.1016/S0167-1987(00)00183-5.
21. Oldeman, L.R. Global extent of soil degradation. In *Bi-Annual Report 1991-1992/ISRIC*; International Soil Reference and Information Centre (ISRIC): Wageningen, Netherlands, 1992; pp. 19–36.
22. Blanco-Canqui, H.; Lal, R. Soil and water conservation. In *Principles of Soil Conservation and Management*; Springer: Berlin/Heidelberg, Germany, 2010; pp. 1-19.
23. Butzer, K.W. Accelerated soil erosion: A problem of man-land relationships. *Perspect. Environ.* **1974**, 57–77.
24. Woodward, J.; Foster, I. Erosion and suspended sediment transfer in river catchments: Environmental controls, processes and problems. *Geography* **1997**, *82*, 353–376.
25. Didone, E.J.; Minella, J.P.G.; Merten, G.H. Quantifying soil erosion and sediment yield in a catchment in southern Brazil and implications for land conservation. *J. Soils Sediments* **2015**, *15*, 2334–2346, https://doi.org/10.1007/s11368-015-1160-0.
26. Keesstra, S.D.; Bouma, J.; Wallinga, J.; Tittonell, P.; Smith, P.; Cerdà, A.; Montanarella, L.; Quinton, J.N.; Pachepsky, Y.; van der Putten, W.H.; et al. The significance of soils and soil science towards realization of the United Nations Sustainable Development Goals. *Soil* **2016**, *2*, 111–128, https://doi.org/10.5194/soil-2-111-2016.
27. Gholami, V.; Sahour, H.; Amri, M.A.H. Soil erosion modeling using erosion pins and artificial neural networks. *Catena* **2021**, *196*, 104902, https://doi.org/10.1016/j.catena.2020.104902.
28. Ashraf, A. Risk modeling of soil erosion under different land use and rainfall conditions in Soan river basin, sub-Himalayan region and mitigation options. *Model. Earth Syst. Environ.* **2019**, *6*, 417–428, https://doi.org/10.1007/s40808-019-00689-6.

29. Boardman, J.; Evans, R. The measurement, estimation and monitoring of soil erosion by runoff at the field scale: Challenges and possibilities with particular reference to Britain. *Prog. Phys. Geogr. Earth Environ.* **2020**, *44*, 31–49, https://doi.org/10.1177%2F0309133319861833.
30. Panagos, P.; Katsoyiannis, A. Soil erosion modelling: The new challenges as the result of policy developments in Europe. *Environ. Res.* **2019**, *172*, 470–474, https://doi.org/10.1016/j.envres.2019.02.043.
31. Rosas, M.; Gutierrez, R.R. Assessing soil erosion risk at national scale in developing countries: The technical challenges, a proposed methodology, and a case history. *Sci. Total Environ.* **2020**, *703*, 135474, https://doi.org/10.1016/j.scitotenv.2019.135474.
32. Bennett, H.H. A Permanent Loss to New England: Soil Erosion Resulting from the Hurricane. *Geogr. Rev.* **1939**, *29*, 196, https://doi.org/10.2307/209942.
33. SMITH, D.D. Interpretation of soil conservation data for field use. *Agric. Eng.* **1941**, *22*, 173–175.
34. Zingg, A.W. Degree and length of land slope as it affects soil loss in run-off. *Agric. Eng.* **1940**, *21*, 59–64.
35. De Vente, J.; Poesen, J. Predicting soil erosion and sediment yield at the basin scale: Scale issues and semi-quantitative models. *Earth-Sci. Rev.* **2005**, *71*, 95–125, https://doi.org/10.1016/j.earscirev.2005.02.002.
36. Jetten, V.; Govers, G.; Hessel, R. Erosion models: Quality of spatial predictions. *Hydrol. Process.* **2003**, *17*, 887–900, https://doi.org/10.1002/hyp.1168.
37. Karydas, C.; Panagos, P.; Gitas, I. A classification of water erosion models according to their geospatial characteristics. *Int. J. Digit. Earth* **2012**, *7*, 229–250, https://doi.org/10.1080/17538947.2012.671380.
38. King, C.; Delpont, G. Spatial assessment of erosion: Contribution of remote sensing, A review. *Remote. Sens. Rev.* **1993**, *7*, 223–232, https://doi.org/10.1080/02757259309532178.
39. Merritt, W.; Letcher, R.; Jakeman, A. A review of erosion and sediment transport models. *Environ. Model. Softw.* **2003**, *18*, 761–799, https://doi.org/10.1016/s1364-8152(03)00078-1.
40. Toy, T.J.; Foster, G.R.; Renard, K.G. *Soil Erosion: Processes, Prediction, Measurement, and Control*; John Wiley & Sons: Hoboken, NJ, USA, 2002.
41. Vrieling, A. Satellite remote sensing for water erosion assessment: A review. *Catena* **2006**, *65*, 2–18, https://doi.org/10.1016/j.catena.2005.10.005.
42. Zhang, L.; O'Neill, A.L.; Lacey, S. Modelling approaches to the prediction of soil erosion in catchments. *Environ. Softw.* **1996**, *11*, 123–133, https://doi.org/10.1016/s0266-9838(96)00023-8.
43. Morgan, R.; Nearing, M. Model development: A user's perspective. In *Handbook of Erosion Modelling*; Blackwell Publishing Ltd.: Hoboken, NJ, USA, 2011; pp. 9–32.
44. Boardman, J. Soil erosion science: Reflections on the limitations of current approaches. *Catena* **2006**, *68*, 73–86, https://doi.org/10.1016/j.catena.2006.03.007.
45. Morgan, R.; Quinton, J.; Smith, R.; Govers, G.; Poesen, J.; Auerswald, K.; Chisci, G.; Torri, D.; Styczen, M. The European Soil Erosion Model (EUROSEM): A dynamic approach for predicting sediment transport from fields and small catchments. *Earth Surf. Process. Landf.* **1998**, *23*, 527–544, https://doi.org/10.1002/(SICI)1096-9837(199806)23:6%3C527::AID-ESP868%3E3.0.CO;2-5.
46. De Roo, A.; Wesseling, C.; Ritsema, C. LISEM: A single-event physically based hydrological and soil erosion model for drainage basins. I: Theory, input and output. *Hydrol. Process.* **1996**, *10*, 1107–1117.
47. Kirkby, M.J.; Irvine, B.J.; Jones, R.J.A.; Govers, G.; Team, P. The PESERA coarse scale erosion model for Europe. I.—Model rationale and implementation. *Eur. J. Soil Sci.* **2008**, *59*, 1293–1306, https://doi.org/10.1111/j.1365-2389.2008.01072.x.
48. Bagarello, V.; Di Piazza, G.; Ferro, V.; Giordano, G. Predicting unit plot soil loss in Sicily, south Italy. *Hydrol. Process. Int. J.* **2008**, *22*, 586–595, https://doi.org/10.1002/hyp.6621.
49. Bagarello, V.; Ferro, V.; Pampalone, V. A new version of the USLE-MM for predicting bare plot soil loss at the Sparacia (South Italy) experimental site. *Hydrol. Process.* **2015**, *29*, 4210–4219, https://doi.org/10.1002/hyp.10486.
50. Bagarello, V.; Ferro, V. Plot-scale measurement of soil erosion at the experimental area of Sparacia (southern Italy). *Hydrol. Process.* **2004**, *18*, 141–157, https://doi.org/10.1002/hyp.1318.
51. Di Stefano, C.; Ferro, V.; Pampalone, V. Testing the USLE-M Family of Models at the Sparacia Experimental Site in South Italy. *J. Hydrol. Eng.* **2017**, *22*, 05017012, https://doi.org/10.1061/(asce)he.1943-5584.0001535.
52. Kinnell, P.I.A. Applying the QREI30index within the USLE modelling environment. *Hydrol. Process*. **2014**, *28*, 591–598, https://doi.org/10.1002/hyp.9591.
53. Cao, L.; Zhang, K.; Dai, H.; Liang, Y. Modeling Interrill Erosion on Unpaved Roads in the Loess Plateau of China. *Land Degrad. Dev.* **2016**, *26*, 825–832, https://doi.org/10.1002/ldr.2253.
54. Gessesse, B.; Bewket, W.; Bräuning, A. Model-Based Characterization and Monitoring of Runoff and Soil Erosion in Response to Land Use/land Cover Changes in the Modjo Watershed, Ethiopia. *Land Degrad. Dev.* **2014**, *26*, 711–724, https://doi.org/10.1002/ldr.2276.
55. Diodato, N.; Borrelli, P.; Fiener, P.; Bellocchi, G.; Romano, N. Discovering historical rainfall erosivity with a parsimonious approach: A case study in Western Germany. *J. Hydrol.* **2017**, *544*, 1–9, https://doi.org/10.1016/j.jhydrol.2016.11.023.
56. Doetterl, S.; Van Oost, K.; Six, J. Towards constraining the magnitude of global agricultural sediment and soil organic carbon fluxes. *Earth Surf. Process. Landforms* **2011**, *37*, 642–655, https://doi.org/10.1002/esp.3198.
57. Van Oost, K.; Quine, T.A.; Govers, G.; De Gryze, S.; Six, J.; Harden, J.W.; Ritchie, J.C.; McCarty, G.W.; Heckrath, G.; Kosmas, C.; et al. The Impact of Agricultural Soil Erosion on the Global Carbon Cycle. *Science* **2007**, *318*, 626–629, https://doi.org/10.1126/science.1145724.

58. Di Stefano, C.; Ferro, V.; Porto, P. Linking Sediment Yield and Caesium-137 Spatial Distribution at Basin Scale. *J. Agric. Eng. Res.* **1999**, *74*, 41–62, https://doi.org/10.1006/jaer.1999.0436.
59. Ferro, V. Further remarks on a distributed approach to sediment delivery. *Hydrol. Sci. J.* **1997**, *42*, 633–647, https://doi.org/10.1080/02626669709492063.
60. Renard, K.G.; Foster, G.R.; Weesies, G.A.; Porter, J.P. RUSLE: Revised universal soil loss equation. *J. Soil Water Conserv.* **1991**, *46*, 30–33.
61. Risse, L.M.; Nearing, M.A.; Laflen, J.M.; Nicks, A.D. Error Assessment in the Universal Soil Loss Equation. *Soil Sci. Soc. Am. J.* **1993**, *57*, 825–833, https://doi.org/10.2136/sssaj1993.03615995005700030032x.
62. Ganasri, B.P.; Ramesh, H. Assessment of soil erosion by RUSLE model using remote sensing and GIS—A case study of Nethravathi Basin. *Geosci. Front.* **2016**, *7*, 953–961, doi:10.1016/j.gsf.2015.10.007.
63. Coen, G.; Tatarko, J.; Martin, T.; Cannon, K.; Goddard, T.; Sweetland, N. A method for using WEPS to map wind erosion risk of Alberta soils. *Environ. Model. Softw.* **2004**, *19*, 185–189, https://doi.org/10.1016/s1364-8152(03)00121-x.
64. Panagos, P.; Meusburger, K.; Van Liedekerke, M.; Alewell, C.; Hiederer, R.; Montanarella, L. Assessing soil erosion in Europe based on data collected through a European network. *Soil Sci. Plant Nutr.* **2014**, *60*, 15–29, https://doi.org/10.1080/00380768.2013.835701.
65. Wall, G.; Coote, D.; Pringle, E.; Shelton, I. *Revised Universal Soil Loss Equation for Application in Canada: A Handbook for Estimating Soil Loss from Water Erosion in Canada*; Agriculture and Agri-Food Canada, Research branch: Ottawa, ON, Canada, 2002.
66. Teng, H.; Rossel, R.A.V.; Shi, Z.; Behrens, T.; Chappell, A.; Bui, E. Assimilating satellite imagery and visible–near infrared spectroscopy to model and map soil loss by water erosion in Australia. *Environ. Model. Softw.* **2016**, *77*, 156–167, https://doi.org/10.1016/j.envsoft.2015.11.024.
67. Wang, X.; Zhao, X.; Zhang, Z.; Yi, L.; Zuo, L.; Wen, Q.; Liu, F.; Xu, J.; Hu, S.; Liu, B. Assessment of soil erosion change and its relationships with land use/cover change in China from the end of the 1980s to 2010. *Catena* **2016**, *137*, 256–268, https://doi.org/10.1016/j.catena.2015.10.004.
68. Wischmeier, W.H.; Smith, D.D. *Predicting Rainfall Erosion Losses: A Guide to Conservation Planning*; Department of Agriculture, Science and Education Administration: Corvallis, OR, USA, 1978.
69. Angima, S.; Stott, D.; O'Neill, M.; Ong, C.; Weesies, G. Soil erosion prediction using RUSLE for central Kenyan highland conditions. *Agric. Ecosyst. Environ.* **2003**, *97*, 295–308, https://doi.org/10.1016/s0167-8809(03)00011-2.
70. Garde, R.; Kathyari, U. Erosion prediction models for large catchments. In Proceedings of the International Symposium on Water Erosion, Sedimentation, and Resource Conservation, Dehradun, India, 9–13 October 1990; pp. 89–102.
71. Millward, A.A.; Mersey, J.E. Adapting the RUSLE to model soil erosion potential in a mountainous tropical watershed. *Catena* **1999**, *38*, 109–129, https://doi.org/10.1016/s0341-8162(99)00067-3.
72. Meyer, L.W.; Wischmeier, W.H. Mathematical simulation of the process of soil erosion by water. *Trans. ASAE* **1969**, *12*, 754–0758.
73. Renard, K.G. *Predicting Soil Erosion by Water: A Guide to Conservation Planning with the Revised Universal Soil Loss Equation (RUSLE)*; United States Government Printing: Washington, DC, USA, 1997.
74. Williams, J. Sediment delivery ratios determined with sediment and runoff models. *IAHS Publ.* **1977**, *122*, 168–179.
75. Woznicki, S.A.; Nejadhashemi, A.P. Spatial and Temporal Variabilities of Sediment Delivery Ratio. *Water Resour. Manag.* **2013**, *27*, 2483–2499, https://doi.org/10.1007/s11269-013-0298-z.
76. Weifeng, Z.; Bingfang, W. Assessment of soil erosion and sediment delivery ratio using remote sensing and GIS: A case study of upstream Chaobaihe River catchment, north China. *Int. J. Sediment Res.* **2008**, *23*, 167–173, https://doi.org/10.1016/S1001-6279(08)60016-5.
77. Renfro, G.W. Use of erosion equations and sediment delivery ratios for predicting sediment yield. In Proceedings of the Sediment yield workshop: Present and prospective technology for predicting sediment yield and sources, Oxford, MS, USA, 1972; pp. 33–45.
78. Ebisemiju, F.S. Sediment delivery ratio prediction equations for short catchment slopes in a humid tropical environment. *J. Hydrol.* **1990**, *114*, 191–208, https://doi.org/10.1016/0022-1694(90)90081-8.
79. Wu, L.; He, Y.; Ma, X. Using five long time series hydrometeorological data to calibrate a dynamic sediment delivery ratio algorithm for multi-scale sediment yield predictions. *Environ. Sci. Pollut. Res.* **2020**, *27*, 16377–16392, https://doi.org/10.1007/s11356-020-08121-8.
80. Saygın, S.D.; Ozcan, A.U.; Basaran, M.; Timur, O.B.; Dolarslan, M.; Yılman, F.E.; Erpul, G. The combined RUSLE/SDR approach integrated with GIS and geostatistics to estimate annual sediment flux rates in the semi-arid catchment, Turkey. *Environ. Earth Sci.* **2013**, *71*, 1605–1618, https://doi.org/10.1007/s12665-013-2565-y.
81. Ebrahimzadeh, S.; Motagh, M.; Mahboub, V.; Harijani, F.M. An improved RUSLE/SDR model for the evaluation of soil erosion. *Environ. Earth Sci.* **2018**, *77*, 454, https://doi.org/10.1007/s12665-018-7635-8.
82. Bhattacharya, R.K.; Das Chatterjee, N.; Das, K. Estimation of Erosion Susceptibility and Sediment Yield in Ephemeral Channel Using RUSLE and SDR Model: Tropical Plateau Fringe Region, India. In Gully erosion studies from India and surrounding regions; Springer: Berlin/Heidelberg, Germany, 2019; pp. 163–185, https://doi.org/10.1007/978-3-030-23243-6_10.
83. de Vente, J.; Poesen, J.; Verstraeten, G.; Van Rompaey, A.; Govers, G. Spatially distributed modelling of soil erosion and sediment yield at regional scales in Spain. *Glob. Planet. Chang.* **2008**, *60*, 393–415, https://doi.org/10.1016/j.gloplacha.2007.05.002.
84. Kamaludin, H.; Lihan, T.; Ali Rahman, Z.; Mustapha, M.; Idris, W.; Rahim, S. Integration of remote sensing, RUSLE and GIS to model potential soil loss and sediment yield (SY). *Hydrol. Earth Syst. Sci. Discuss.* **2013**, *10*, 4567–4596.

85. Cerdan, O.; Govers, G.; Le Bissonnais, Y.; Van Oost, K.; Poesen, J.; Saby, N.; Gobin, A.; Vacca, A.; Quinton, J.; Auerswald, K.; et al. Rates and spatial variations of soil erosion in Europe: A study based on erosion plot data. *Geomorphology* **2010**, *122*, 167–177, https://doi.org/10.1016/j.geomorph.2010.06.011.
86. Ali, S.; Cheema, M.J.M.; Waqas, M.M.; Waseem, M.; Leta, M.K.; Qamar, M.U.; Awan, U.K.; Bilal, M.; Rahman, M.H.U. Flood Mitigation in the Transboundary Chenab River Basin: A Basin-Wise Approach from Flood Forecasting to Management. *Remote Sens.* **2021**, *13*, 3916, https://doi.org/10.3390/rs13193916.
87. Safari, Z.; Rahimi, S.; Ahmed, K.; Sharafati, A.; Ziarh, G.; Shahid, S.; Ismail, T.; Al-Ansari, N.; Chung, E.-S.; Wang, X. Estimation of Spatial and Seasonal Variability of Soil Erosion in a Cold Arid River Basin in Hindu Kush Mountainous Region Using Remote Sensing. *Sustainability* **2021**, *13*, 1549, https://doi.org/10.3390/su13031549.
88. Ali, S.; Cheema, M.; Waqas, M.; Waseem, M.; Awan, U.; Khaliq, T. Changes in Snow Cover Dynamics over the Indus Basin: Evidences from 2008 to 2018 MODIS NDSI Trends Analysis. *Remote. Sens*. **2020**, *12*, 2782, https://doi.org/10.3390/rs12172782.
89. Ali, S.; Cheema, M.J.M.; Bakhsh, A.; Khaliq, T. Near Real Time Flood Forecasting in the Transboundary Chenab River Using Global Satellite Mapping of Precipitation. *Pak. J. Agric. Sci.* **2020**, *57*, 1327–1335.
90. Williams, J. Sediment routing for agricultural watersheds. *JAWRA J. Am. Water Resour. Assoc.* **1975**, *11*, 965–974, https://doi.org/10.1111/j.1752-1688.1975.tb01817.x.
91. Evans, M.; Lindsay, J. High resolution quantification of gully erosion in upland peatlands at the landscape scale. *Earth Surf. Process. Landf.* **2010**, *35*, 876–886, https://doi.org/10.1002/esp.1918.
92. Onnen, N.; Heckrath, G.; Stevens, A.; Olsen, P.; Greve, M.B.; Pullens, J.W.; Kronvang, B.; Van Oost, K. Distributed water erosion modelling at fine spatial resolution across Denmark. *Geomorphology* **2019**, *342*, 150–162, https://doi.org/10.1016/j.geomorph.2019.06.011.
93. Ismail, J.; Ravichandran, S. RUSLE2 Model Application for Soil Erosion Assessment Using Remote Sensing and GIS. *Water Resour. Manag.* **2007**, *22*, 83–102, https://doi.org/10.1007/s11269-006-9145-9.
94. Lu, D.; Li, G.; Valladares, G.S.; Batistella, M. Mapping soil erosion risk in Rondonia, Brazilian Amazonia: Using RUSLE, remote sensing and GIS. *Land Degrad. Dev.* **2004**, *15*, 499–512, https://doi.org/10.1002/ldr.634.
95. Aiello, A.; Adamo, M.; Canora, F. Remote sensing and GIS to assess soil erosion with RUSLE3D and USPED at river basin scale in southern Italy. *Catena* **2015**, *131*, 174–185, https://doi.org/10.1016/j.catena.2015.04.003.
96. Alkharabsheh, M.; Alexandridis, T.; Bilas, G.; Misopolinos, N.; Silleos, N. Impact of Land Cover Change on Soil Erosion Hazard in Northern Jordan Using Remote Sensing and GIS. *Procedia Environ. Sci.* **2013**, *19*, 912–921, https://doi.org/10.1016/j.proenv.2013.06.101.
97. Kouli, M.; Soupios, P.; Vallianatos, F. Soil erosion prediction using the Revised Universal Soil Loss Equation (RUSLE) in a GIS framework, Chania, Northwestern Crete, Greece. *Environ. Geol.* **2009**, *57*, 483–497, https://doi.org/10.1007/s00254-008-1318-9.
98. Rao, S.V.N.; Rao, M.V.; Ramasastri, K.S.; Singh, R.N.P. A Study of Sedimentation in Chenab Basin in Western Himalayas. *Hydrol. Res.* **1997**, *28*, 201–216, https://doi.org/10.2166/nh.1997.0012.
99. Amin, M.; Romshoo, S.A. Comparative assessment of soil erosion modelling approaches in a Himalayan watershed. *Model. Earth Syst. Environ.* **2018**, *5*, 175–192, https://doi.org/10.1007/s40808-018-0526-x.
100. Romshoo, S.A.; Altaf, S.; Amin, M.; Ameen, U. Sediment yield estimation for developing soil conservation strategies in GIS environment for the mountainous Marusudar catchment, Chenab basin, J&K, India. *J. Himal. Ecol. Sustain. Dev.* **2017**, *12*, 16–32.
101. Singh, P.; Ramasastri, K.S.; Kumar, N. Topographical Influence on Precipitation Distribution in Different Ranges of Western Himalayas. *Hydrol. Res.* **1995**, *26*, 259–284, https://doi.org/10.2166/nh.1995.0015.
102. Leta, M.; Demissie, T.; Tränckner, J. Modeling and Prediction of Land Use Land Cover Change Dynamics Based on Land Change Modeler (LCM) in Nashe Watershed, Upper Blue Nile Basin, Ethiopia. *Sustainability* **2021**, *13*, 3740, https://doi.org/10.3390/su13073740.
103. Singh, S.K.; Srivastava, P.K.; Gupta, M.; Thakur, J.K.; Mukherjee, S. Appraisal of land use/land cover of mangrove forest ecosystem using support vector machine. *Environ. Earth Sci.* **2013**, *71*, 2245–2255, https://doi.org/10.1007/s12665-013-2628-0.
104. Koneti, S.; Sunkara, S.L.; Roy, P.S. Hydrological Modeling with Respect to Impact of Land-Use and Land-Cover Change on the Runoff Dynamics in Godavari River Basin Using the HEC-HMS Model. *ISPRS Int. J. Geo-Inf.* **2018**, *7*, 206, https://doi.org/10.3390/ijgi7060206.
105. Dwarakish, G.; Ganasri, B. Impact of land use change on hydrological systems: A review of current modeling approaches. *Cogent Geosci.* **2015**, *1*, 1115691, https://doi.org/10.1080/23312041.2015.1115691.
106. Leta, M.K.; Demissie, T.A.; Tränckner, J. Hydrological Responses of Watershed to Historical and Future Land Use Land Cover Change Dynamics of Nashe Watershed, Ethiopia. *Water* **2021**, *13*, 2372, https://doi.org/10.3390/w13172372.
107. ESA. European Space Agency. Land Cover CCI Product User Guide Version 2. Tech. Rep. (2017). Available online: Maps.elie.ucl.ac.be/CCI/viewer/download/ESACCI-LC-Ph2-PUGv2_2.0.pdf. 2017 (accessed on: 19 November 2008).
108. Srivastava, P.K.; Han, D.; Rico-Ramirez, M.A.; O'Neill, P.; Islam, T.; Gupta, M. Assessment of SMOS soil moisture retrieval parameters using tau–omega algorithms for soil moisture deficit estimation. *J. Hydrol.* **2014**, *519*, 574–587, https://doi.org/10.1016/j.jhydrol.2014.07.056.
109. Yang, D.; Gao, B.; Jiao, Y.; Lei, H.; Zhang, Y.; Yang, H.; Cong, Z. A distributed scheme developed for eco-hydrological modeling in the upper Heihe River. *Sci. China Earth Sci.* **2015**, *58*, 36–45, https://doi.org/10.1007/s11430-014-5029-7.
110. Renard, K.; Foster, G.; Weesies, G.; McCool, D.; Yoder, D. Predicting soil erosion by water: A guide to conservation planning with the Revised Universal Soil Loss Equation (RUSLE). *Agric. Handb.* **1996**, *703*, 25–28.

111. Morgan, R.P.C.; Quinton, J.; Rickson, R.J. Modelling Methodology for Soil Erosion Assessment and Soil Conservation Design: The EUROSEM Approach. *Outlook Agric.* **1994**, *23*, 5–9, https://doi.org/10.1177/003072709402300103.
112. Jung, P.-K.; Ko, M.-H.; Im, J.-N.; Um, K.-T.; Choi, D.-U. Rainfall erosion factor for estimating soil loss. *Korean J. Soil Sci. Fertil.* **1983**, *16*, 112–118.
113. Sharpley, A.N.; Williams, J.R. EPIC. Erosion/Productivity impact calculator: 1. Model documentation. 2. User manual. EPIC: Cary, NC, USA 1990.
114. Beskow, S.; de Mello, C.; Norton, L.; Curi, N.; Viola, M.R.; Avanzi, J. Soil erosion prediction in the Grande River Basin, Brazil using distributed modeling. *Catena* **2009**, *79*, 49–59, https://doi.org/10.1016/j.catena.2009.05.010.
115. Pal, S.C.; Shit, M. Application of RUSLE model for soil loss estimation of Jaipanda watershed, West Bengal. *Spat. Inf. Res.* **2017**, *25*, 399–409, https://doi.org/10.1007/s41324-017-0107-5.
116. Pandey, A.; Chowdary, V.M.; Mal, B.C. Identification of critical erosion prone areas in the small agricultural watershed using USLE, GIS and remote sensing. *Water Resour. Manag.* **2007**, *21*, 729–746, https://doi.org/10.1007/s11269-006-9061-z.
117. Karaburun, A. Estimation of C factor for soil erosion modeling using NDVI in Buyukcekmece watershed. *Ozean J. Appl. Sci.* **2010**, *3*, 77–85.
118. Kayet, N.; Pathak, K.; Chakrabarty, A.; Sahoo, S. Urban heat island explored by co-relationship between land surface temperature vs multiple vegetation indices. *Spat. Inf. Res.* **2016**, *24*, 515–529, https://doi.org/10.1007/s41324-016-0049-3.
119. Julien, P.Y. *Erosion and Sedimentation*; Cambridge University Press: Cambridge, UK, 2010.
120. Van Rompaey, A.J.J.; Verstraeten, G.; Van Oost, K.; Govers, G.; Poesen, J. Modelling mean annual sediment yield using a distributed approach. *Earth Surf. Process. Landf.* **2001**, *26*, 1221–1236, https://doi.org/10.1002/esp.275.
121. USDA, S. *National Engineering Handbook*; Section 4: Hydrology; U.S. Department of Agriculture: Washington, DC, USA, 1972.
122. Klaghofer, E.; Summer, W.; Villeneuve, J. Some remarks on the determination of the sediment delivery ratio. *Int. Assoc. Hydrol. Sci. Publ.* **1992**, *209*, 113–118.
123. Roehl, J. *Sediment Source Areas, Delivery Ratios and Influencing Morphological Factors*; Internation Association for Scientific Hydrology Commission of Land Erosion: 1962.
124. Vanoni, V.A. Sediment Deposition Engineering. In *ASCE Manuals and Reports on Engineering Practices, No. 54*; American Society of Civil Engineers: Reston, VA, USA, 1975.
125. Bazzoffi, P.; Baldassarre, G.; Vacca, S. Validation of PISA2 model for automatic assessment of reservoir sedimentation. In Proceedings of the International Conference on Reservoir Sedimentation; Albertson, M., Ed.; Colorado State University: Fort Collins, CO, USA, 1996; pp. 519-528.
126. Williams, J.R.; Berndt, H.D. Sediment Yield Prediction Based on Watershed Hydrology. *Trans. ASAE* **1977**, *20*, 1100–1104, https://doi.org/10.13031/2013.35710.
127. Panagos, P.; Borrelli, P.; Poesen, J.; Meusburger, K.; Ballabio, C.; Lugato, E.; Montanarella, L.; Alewell, C. Reply to "The new assessment of soil loss by water erosion in Europe. Panagos P. et al., 2015 Environ. Sci. Policy 54, 438–447—A response" by Evans and Boardman [Environ. Sci. Policy 58, 11–15]. *Environ. Sci. Policy* **2016**, *59*, 53–57, https://doi.org/10.1016/j.envsci.2016.02.010.
128. Shin, G. The Analysis of Soil Erosion Analysis in Watershed using GIS. Ph. D. Thesis, Department of Civil Engineering, Gangwon National University, Gangwon-do, Korea, 1999.
129. Singh, G.; Babu, R.; Narain, P.; Bhushan, L.; Abrol, I. Soil erosion rates in India. *J. Soil Water Conserv.* **1992**, *47*, 97–99.
130. Maqsoom, A.; Aslam, B.; Hassan, U.; Kazmi, Z.A.; Sodangi, M.; Tufail, R.F.; Farooq, D. Geospatial Assessment of Soil Erosion Intensity and Sediment Yield Using the Revised Universal Soil Loss Equation (RUSLE) Model. *ISPRS Int. J. Geo-Inf.* **2020**, *9*, 356, https://doi.org/10.3390/ijgi9060356.
131. Walling, D. Erosion and sediment yield research—some recent perspectives. *J. Hydrol.* **1988**, *100*, 113–141, Erosion and sediment yield research—Some recent perspectives.
132. Morgan, R.P.C. *Soil Erosion and Conservation*; John Wiley & Sons: Hoboken, NJ, USA, 2009.
133. Bai, L.; Shi, C.; Li, L.; Yang, Y.; Wu, J. Accuracy of CHIRPS Satellite-Rainfall Products over Mainland China. *Remote Sens.* **2018**, *10*, 362, https://doi.org/10.3390/rs10030362.
134. Haan, C.T.; Barfield, B.J.; Hayes, J.C. *Design Hydrology and Sedimentology for Small Catchments*; Elsevier: Amsterdam, The Netherlands, 1994.
135. Ullah, S.; Ali, A.; Iqbal, M.; Javid, M.; Imran, M. Geospatial assessment of soil erosion intensity and sediment yield: A case study of Potohar Region, Pakistan. *Environ. Earth Sci.* **2018**, *77*, 705, https://doi.org/10.1007/s12665-018-7867-7.
136. Gajbhiye, S.; Mishra, S.K.; Pandey, A. Simplified sediment yield index model incorporating parameter curve number. *Arab. J. Geosci.* **2014**, *8*, 1993–2004, https://doi.org/10.1007/s12517-014-1319-9.
137. Mutua, B.M.; Klik, A. Estimating spatial sediment delivery ratio on a large rural catchment. *J. Spat. Hydrol.* **2006**, *6*, 1.
138. Lee, S.E.; Kang, S.H. Geographic information system-coupling sediment delivery distributed modeling based on observed data. *Water Sci. Technol.* **2014**, *70*, 495–501, https://doi.org/10.2166/wst.2014.231.
139. Lu, H.; Moran, C.; Prosser, I.P. Modelling sediment delivery ratio over the Murray Darling Basin. *Environ. Model. Softw.* **2006**, *21*, 1297–1308, https://doi.org/10.1016/j.envsoft.2005.04.021.
140. Diodato, N.; Grauso, S. An improved correlation model for sediment delivery ratio assessment. *Environ. Earth Sci.* **2009**, *59*, 223–231, https://doi.org/10.1007/s12665-009-0020-x.

141. Lu, H.; Moran, C.; Sivapalan, M. A theoretical exploration of catchment-scale sediment delivery. *Water Resour. Res.* **2005**, *41*, https://doi.org/10.1029/2005WR004018.
142. Heckmann, T.; Vericat, D. Computing spatially distributed sediment delivery ratios: Inferring functional sediment connectivity from repeat high-resolution digital elevation models. *Earth Surf. Process. Landf.* **2018**, *43*, 1547–1554, https://doi.org/10.1002/esp.4334.
143. Park, Y.; Kim, J.; Kim, N.; Kim, K.-S.; Choi, J.; Lim, K.J. Analysis of sediment yields at watershed scale using area/slope-based sediment delivery ratio in SATEEC. *J. Korean Soc. Water Environ.* **2007**, *23*, 650–658.
144. Pelletier, J.D. A spatially distributed model for the long-term suspended sediment discharge and delivery ratio of drainage basins. *J. Geophys. Res. Earth Surf.* **2012**, *117*, https://doi.org/10.1029/2011jf002129.
145. Ferro, V.; Minacapilli, M. Sediment delivery processes at basin scale. *Hydrol. Sci. J.* **1995**, *40*, 703–717, https://doi.org/10.1080/02626669509491460.
146. Brasington, J.; Richards, K. Interactions between model predictions, parameters and DTM scales for topmodel. *Comput. Geosci.* **1998**, *24*, 299–314, https://doi.org/10.1016/s0098-3004(97)00081-2.
147. Gao, J. Impact of sampling intervals on the reliability of topographic variables mapped from grid DEMs at a micro-scale. *Int. J. Geogr. Inf. Sci.* **1998**, *12*, 875–890, https://doi.org/10.1080/136588198241545.
148. Zhang, X.; Drake, N.A.; Wainwright, J.; Mulligan, M. Comparison of slope estimates from low resolution DEMs: Scaling issues and a fractal method for their solution. *Earth Surf. Process. Landf.* **1999**, *24*, 763–779, https://doi.org/10.1002/(SICI)1096-9837(199908)24:9%3C763::AID-ESP9%3E3.0.CO;2-J.
149. Rajbanshi, J.; Bhattacharya, S. Assessment of soil erosion, sediment yield and basin specific controlling factors using RUSLE-SDR and PLSR approach in Konar river basin, India. *J. Hydrol.* **2020**, *587*, 124935, https://doi.org/10.1016/j.jhydrol.2020.124935.
150. Gelagay, H.S. RUSLE and SDR Model Based Sediment Yield Assessment in a GIS and Remote Sensing Environment; A Case Study of Koga Watershed, Upper Blue Nile Basin, Ethiopia. *Gelagay Hydrol. Curr. Res.* **2016**, *7*, 2, https://doi.org/10.4172/2157-7587.1000239.
151. Thomas, J.; Joseph, S.; Thrivikramji, K.P. Assessment of soil erosion in a monsoon-dominated mountain river basin in India using RUSLE-SDR and AHP. *Hydrol. Sci. J.* **2018**, *63*, 542–560, https://doi.org/10.1080/02626667.2018.1429614.
152. Behera, M.; Sena, D.R.; Mandal, U.; Kashyap, P.S.; Dash, S.S. Integrated GIS-based RUSLE approach for quantification of potential soil erosion under future climate change scenarios. *Environ. Monit. Assess.* **2020**, *192*, 1–18, https://doi.org/10.1007/s10661-020-08688-2.
153. Swarnkar, S.; Malini, A.; Tripathi, S.; Sinha, R. Assessment of uncertainties in soil erosion and sediment yield estimates at ungauged basins: An application to the Garra River basin, India. *Hydrol. Earth Syst. Sci.* **2018**, *22*, 2471–2485, https://doi.org/10.5194/hess-22-2471-2018.
154. Gashaw, T.; Tulu, T.; Argaw, M.; Worqlul, A.W. Modeling the impacts of land use–land cover changes on soil erosion and sediment yield in the Andassa watershed, upper Blue Nile basin, Ethiopia. *Environ. Earth Sci.* **2019**, *78*, 1–22, https://doi.org/10.1007/s12665-019-8726-x.
155. Anees, M.T.; Abdullah, K.; Nawawi, M.N.M.; Norulaini, N.A.N.; Syakir, M.I.; Omar, A.K.M. Soil erosion analysis by RUSLE and sediment yield models using remote sensing and GIS in Kelantan state, Peninsular Malaysia. *Soil Res.* **2018**, *56*, 356, https://doi.org/10.1071/sr17193.
156. Fistikoglu, O.; Harmancioglu, N.B. Integration of GIS with USLE in Assessment of Soil Erosion. *Water Resour. Manag.* **2002**, *16*, 447–467, https://doi.org/10.1023/a:1022282125760.
157. Nasir, A.; Uchida, K.; Ashraf, M. Estimation of soil erosion by using RUSLE and GIS for small mountainous watersheds in Pakistan. *Pak. J. Water Resour.* **2008**, 10, 11–21.